Tungsten (2020) 2:261–288
https://doi.org/10.1007/s42864-020-00057-3

Tungsten
www.springer.com/42864

REVIEW PAPER

Synthesis of cobalt, palladium, and rhenium nanoparticles

Shahab Ranjbar Bahadori[1] · Ryan Hart[1] · Yao-Wu Hao[1]

Received: 28 May 2020 / Revised: 18 July 2020 / Accepted: 20 July 2020 / Published online: 11 September 2020

Abstract
Over the past decade, metal nanoparticles (MNPs) have attracted extensive attention due to their unique physiochemical properties that make them highly applicable in various fields such as chemical sensing, energy storage, catalysis, medicine, and environmental engineering. Their physiochemical properties depend drastically on the MNP size and morphology, which are largely determined by their synthesis methods. Research on MNPs predominantly focused on coinage metals (Au, Ag and Cu), but in the last decade research on metals with a relatively high melting temperature such as Pd, Co, and Re has seen rapid increases, mainly driven by their potential applications as catalysts. This paper presents the recent advances on different synthesis techniques of Co, Pd, and Re nanoparticles, their resulting nanostructures, as well as existing and potential applications.

Keywords Nanotechnology · Co nanoparticle · Pd nanoparticle · Re nanoparticle · Nanoparticle synthesis

1 Introduction

Nanotechnology has gained widespread attention since it was presented by Nobel laureate Feynman [1] during his famous 1959 lecture "There's plenty of room at the bottom" [2]. Nanomaterials, or materials which include at least one dimension (length, width, thickness) within the range of 1–100 nm [3], are considered as a bridge between atomic structures and bulk materials. They exhibit very different physical, chemical, and biological properties from their bulk counterparts such as melting point, wettability, electrical and thermal conductivity, catalytic activity, and light absorption and scattering, which provide new building blocks for various applications [4]. Based on the physical and chemical properties, nanoparticles (NPs) can be classified into carbon-based NPs, ceramic NPs, semiconductor NPs, polymeric NPs, and metal NPs [2]. Among these, metal nanoparticles (MNPs) exhibit exclusive physiochemical properties such as high stability, simple synthesis, exceptional optical properties and catalytic activities, and tunable surface functionalization [5–7], and have thus shown promise for myriad applications in catalysis, environmental sensing, biosensing, medicine, water purification, etc. [8–10].

In the scientific arena, the first literature on MNPs was reported by Michael Faraday, who synthesized colloidal AuNPs in 1857 [4]. As research on MNPs drastically expanded, MNP synthesis approaches can largely be classified into top-down and bottom-up strategies [11–13]. In top-down techniques, the bulk metal is converted via various chemical, mechanical, or physical methods to a nanoscale structure, including mechanical milling, thermal, laser ablation, etc. In contrast, the bottom-up approach employs atoms or molecules as starting materials to join and construct desired MNPs. This approach includes methods such as physical and chemical vapor deposition, sol–gel, solvothermal, chemical reduction, spray pyrolysis, microwave-assisted solution synthesis techniques, etc.[14].

This review concentrates on three high melting temperature transition metals: Co, Pd, and Re. Co has high Curie temperature of about 1131 °C, making it applicable in a broad temperature range [15, 16]. Moreover, Co exhibits exceptional magnetic, electronic, and chemical properties and is one of the first nonprecious metal used as catalysts [17]. MNPs are known as the proper choice for catalytic activities because of their relatively large surface area per volume [18] and possess large numbers of catalytically active atoms on certain crystallographic planes which usually favors small MNPs. Cobalt nanoparticles (CoNPs) are

✉ Yao-Wu Hao
yhao@uta.edu

[1] Department of Materials Science and Engineering, University of Texas at Arlington, Arlington, TX 76019, USA

considered as a good replacement for noble metals due to their availability, lower cost, and sometimes even high activity [19, 20]. Due to their high magnetic coercivity, CoNPs are employed in various electro-magnetic devices, especially in magnetic recording media [21, 22]. The magnetic properties of CoNPs are determined by various parameters including chemical composition, crystal structure, degree of its defectiveness, and interaction of nanoparticles with the surrounding matrix influence [23]. Pd is a precious metal belongs to the platinum group [24]. Though it is mostly used as catalyst, it is also implemented in other industries such as electronic, biomedical, and jewelry [25, 26]. Palladium nanoparticles (PdNPs) which exhibit extensive catalytic potential [27], are used for the wide range of catalytic applications such as hydrogenation [28, 29], oxidation [30, 31], carbon–carbon bond formation [32], and electrochemical reactions in fuel cells [33]. Size and shape of nanoparticles as well as species adsorbed on surface of nanoparticles define the catalytic properties of nanoparticles [34–36]. Among all metals, Re has the second-highest melting point of 3185 °C [37]. Its superior electrical and thermal characteristics make it a viable candidate for electrical applications such as electrodes, electromagnets, sensors, and thermocouples [38, 39]. In addition, it is a vital component of superalloys employed in space and aviation industries. Due to their exceptional mechanical properties as well as outstanding resistant to corrosion and oxidation even at elevated temperature, rhenium nanoparticles (ReNPs) are popular in electronics and catalytic applications [39–41].

2 Metal cobalt nanoparticles

CoNPs are explored for a wide range of applications including catalysts [42], sensors [43], magnetic resonance imaging (MRI) probes [23], and antibacterial agents [44]. Various techniques are employed to synthesize CoNPs, which are listed in detail in Table 1.

2.1 Pure cobalt nanoparticles

One of the conventional synthesis methods for CoNPs is a chemical reduction, in which an ionic precursor is reduced by various kinds of reducing agents in the presence of a surfactant to stabilize the final NPs [89]. Medvedeva et al. [23] synthesized CoNPs through dissolving hyperbranched polyester polyol (HBPO) Boltorn H20 (BH20) as the precursor in 50% water–ethanol (EtOH) and adding a Cobalt (II) chloride ($CoCl_2$) precursor with different Co^{2+}:HBPO molar ratios. The solution was stirred for 12 h and then cooled to 4 °C, followed by addition of sodium borohydride ($NaBH_4$) dropwise during stirring. Microstructure examinations of dried and washed CoNPs demonstrated that the highest stability was achieved with a $CoCl_2$:HBPO molar ratio of 12:1. Moreover, the resultant NPs exhibited superparamagnetic properties at room temperature. In a similar study, Silva et al. [45] made CoNPs by replacing HBPO BH20 stabilizer with oleic acid. The analysis confirmed that increasing the reductant and stabilizer concentration resulted in a high reaction rate, and in turn a small NP size. It is worth noting that later experiments showed NPs synthesized using this method contained cobalt oxide (CoO) [46].

Synthesis of CoNPs through chemical reduction approach is possible even without utilizing a polymeric substance as a surfactant. Kudlash et al. [47] synthesized CoNPs in the absence of a polymeric stabilizer by employing the interphase reduction of cobalt oleate ($C_{36}H_{66}CoO_4$, hexane or toluene solution) and $NaBH_4$ (aqueous or EtOH solution). The X-ray diffraction (XRD) pattern showed no oxide peaks, suggesting that hexane (toluene) or sodium oleate could possibly develop a protective layer on the surface of CoNPs, which protects them against oxidation. Alex et al. [48] obtained CoNPs by reducing cobalt sulfate ($CoSO_4$) with hydrazine (N_2H_4). In this method, high concentrations of N_2H_4 gave rise to small CoNPs while the low concentrations transformed the spherical CoNPs to dendrite ones. Furthermore, the addition of citric acid can increase the reducing power of N_2H_4 [49]. Swain et al. [50] tried to commercialize CoNPs production by reducing $CoSO_4$ in a pilot plant. First, $CoSO_4.7H_2O$ was mixed with concentrated hydrochloric acid (HCl) to produce $CoCl_2$, and then sodium hydroxide (NaOH) was added to obtain cobalt hydroxide ($Co(OH)_2$) precipitate, followed by reducing with 50% hypophosphorous acid (H_3PO_2) solution under stirring at room temperature. Finally, the washed CoNPs were kept under vacuum for 12 h at a temperature of 60 °C to dry. Microstructure examination illustrated that the CoNPs morphology and mean size is dependent on the NaOH concentration, where low NaOH concentrations resulted in small spherical NPs, and high NaOH concentrations created big disk-shape NPs.

In another chemical reduction process, hydrogen is used to replace aqueous reductants to produce metal nanopowders from their oxides [90]. Jang et al. [51] synthesized CoNPs by hydrogen reduction in gas phase using multistage tubular aerosol flow reactor. The reactor design included three sections: evaporation, preheating, and reaction. First, $CoCl_2$ powder was heated at 400 °C and an argon (Ar) flow transferred the resultant $CoCl_2$ vapor into the inner tube positioned inside the preheating section at a temperature of 800–900 °C. A separate tube was used for the H_2 flow. The chemical reactions took place at the exit of nozzles located between preheating and reaction sections at 800–950 °C. When the temperature at the preheating zone was less than that of the reaction zone, the CoNPs size decreased but with a less uniform size distribution. Furthermore, by increasing the fraction of $CoCl_2$, the NP growth dominated the

Table 1 Synthesis of CoNPs through various techniques

NP type	Synthesis method	Function	Size (nm)	Shape	References
CoNPs	Chemical reduction	Potential MRI agent	8.2 ± 3.4	Sphere	[23]
CoNPs	Chemical reduction	–	4–72	Sphere	[45]
CoNPs	Chemical reduction	Removal of organic dyes from wastewater	5–10	Sphere	[46]
CoNPs	Chemical reduction	–	4–7	Sphere	[47]
CoNCs	Chemical reduction	–	30–70	Sphere	[48]
CoNPs	Chemical reduction	–	400	Sphere and dendrite	[49]
CoNPs	Chemical reduction	–	100–300	Sphere and disk	[50]
CoNPs	Hydrogen reduction	–	50–78	Sphere	[51, 52]
CoNPs	Hydrogen reduction	–	43	Sphere	[53]
Carbon-coated CoNPs	Hydrogen reduction	–	72–80	Sphere	[54]
Carbon-coated CoNPs	Hydrogen reduction	Potential applications in separation, sensing, and biomedical devices	29 ± 9	Sphere	[43]
CoNPs	Liquid-phase plasma reduction	–	10–100	Sphere and acicula	[55]
CoNPs	Hydrothermal	–	10–30	Undefined	[56]
CoNPs	Hydrothermal	Potential biomedical applications	200–600	Sphere	[57]
CoNPs	Solvothermal	Catalyst for glycerol hydrogenolysis	500	Sphere	[58]
			10 (diameter)	Rod	
CoNPs	Solvothermal	–	6–40	Cube and sphere	[59]
CoNPs	Thermal decomposition	–	6–8	Sphere	[60]
CoNPs	Thermal decomposition	–	10 ± 1.1	Sphere	[61]
CoNPs	Thermal decomposition	–	25–40	Sphere and disk	[62]
CoNPs	Thermal decomposition	–	10–20	Sphere	[63]
CoNPs	Thermal decomposition	Charge storage floating gate for NVM	5	Sphere	[64]
CoNPs	Thermal decomposition	–	15–25	Sphere	[65]
CoNPs	Thermal decomposition	–	12–15	Sphere	[66]
CoNCs	Thermal decomposition	–	50	Cube	[67]
	Thermal decomposition		7.2 ± 1.7	Sphere	
CoNPs	Polyol	–	7.1 ± 1.0	Undefined	[68]
	Chemical reduction		6.2 ± 1.0	Sphere	
CoNPs	Electrodeposition	Catalysts support in ethanol reforming	110–240	Sphere	[69]
CoNPs	Flame spray pyrolysis	–	30	Sphere	[70]
Co@C NPs	Flame spray pyrolysis	Magnetic separations in organic synthesis	50	Sphere	[71]
Co@C NPs	Flame spray pyrolysis	–	5–50	Sphere	[72]
CoNPs	Ultrasonic spray pyrolysis	–	480–596	Sphere	[73]
CoNPs	Ultrasonic spray pyrolysis	–	55–270	Sphere	[74]
CoNPs	Ion sputtering	–	A few-100	Sphere	[75]
CoNPs	Ion implantation	–	1.5–10	Sphere	[76]
CoNPs	Ion implantation	–	20–25	Sphere	[77]
CoNPs	Arc discharge	–	13.18 ± 3	Sphere	[78]
CoNPs	Pulsed laser ablation	–	8–96	Sphere	[79]
CoNPs	Pulsed wire evaporation	–	< 50	Sphere	[80]
CoNPs	Biogenic	Potential ascorbic acid sensor	–	–	[81]
CoNPs	Biogenic	Potential antibacterial applications	20–49	Cube and hexagon	[82]

Table 1 (continued)

NP type	Synthesis method	Function	Size (nm)	Shape	References
CoNPs	Biogenic	Antibacterial against Gram-negative bacteria	48	Sphere	[44]
CoNPs	Biogenic	–	20–60	Sphere	[83]
Co@GO NSs	Code position and thermal treatment/Hydrothermal	Catalytic degradation of Orange II	29.9	Sphere	[42]
Co@Graphene nanocomposite	Liquid-phase plasma reduction	–	2–7	Sphere	[84]
Co@PE NPs	Thermal decomposition	Magnetic recording applications	4	Sphere	[85, 86]
Co@N-CNTs	Thermal decomposition	Catalysis of ORR	100 nm (diameter)	Cylinder	[87]
Co@N-CNTs	Thermal decomposition	Catalyst for ORR and OER	200 (diameter)	Cylinder	[88]

CoNCs cobalt nanocubes, *CoNSs* cobalt nanosheets, *PE* polyethylene, *GO* graphene oxide, *Co@NC NTs* cobalt encapsulated with nitrogen-doped carbon nanotubes, *ORR* oxygen reduction reaction, *OER* oxygen evolution reaction, *NVM* non-volatile memory

sintering, resulting in large CoNPs [52]. Dzidziguri et al. [53] synthesized CoNPs via a two-step method involving calcination followed by hydrogen reduction. First, a mixture of cobalt(II) nitrate hexahydrate ($Co(NO_3)_2{\cdot}6H_2O$) in alkali solution of NaOH with pH adjusted to ~ 8–9 was fed into the reactor at 10 °C and centrifuged at 700 $r{\cdot}min^{-1}$ to produce $Co(OH)_2$. Then, washed cobalt hydroxide was lyophilized, followed by calcination in the muffle furnace at 400 °C to obtain cobalt oxide. The resulting oxide was reduced via hydrogen flow at 220 °C in a quartz reactor for 30–150 min, producing CoNPs. According to the microstructure analysis, the mean size of CoNPs was not affected by the reducing time, but the number of NPs increased linearly with the reduction time. Hydrogen reduction can also be used for in situ functionalization of CoNPs. Koskela et al. [54] functionalized CoNPs with carbon by introducing ethene to the reaction flow. Carbon coating significantly decreased the average diameter of CoNPs. In addition, it acted as a protective layer against Co leakage and oxidation in acidic solutions. These carbon-coated CoNPs could be functionalized with 3-aminopropyltriethoxysilane (APTES) and 3-mercaptopropyltrimethoxysilane (MPTS) for biological applications [43].

Kim et al. [55] employed liquid-phase plasma (LPP) reduction to synthesize CoNPs. In LPP, large quantities of electrons are created, which facilitate the reduction of metal ions to metal, forming NPs suspension [91]. An aqueous solution of $CoCl_2$ was mixed with the surfactant of sodium dodecyl sulfate (SDS) to prevent agglomeration, and then the resultant solution was transferred into the reactor and, consequently, reduced by a pulsed electrical plasma discharge generated by a high-frequency bipolar pulse power supply. LPP reduction allowed the reduction of metal ions without using reductants since the plasma in liquid phase provided a reaction field with a highly excited energy state. It was demonstrated that reducing the SDS concentration increased the mean size of CoNPs. Similarly, the size uniformity of NPs was improved by increasing the plasma treatment time from 10 to 30 min. However, long plasma treatment changed the morphology of spherical CoNPs to acicular ones.

Another approach for MNPs production is hydrothermal synthesis, defined as a series of reactions in aqueous media at temperatures above 100 °C and 10^5 Pa [92, 93]. Seong et al. [56] employed supercritical hydrothermal reduction to produce CoNPs. A mixture of the cobalt(II) acetate tetrahydrate ($C_4H_6CoO_4{\cdot}4H_2O$) (the precursor) and formic acid (CH_2O_2) (reducing agent) was heated at 340–420 °C for 10 min inside an electric furnace under Ar atmosphere. Then, the batch reactor was placed in a water bath (~ 25 °C) for 5 min to prevent the growth of NPs, and the resultant CoNPs were collected by adding methanol to the reactor (Eqs. (1)–(3)):

$$Co(acetate)_2 + xH_2O \leftrightarrow CO(OH)_x \leftrightarrow CoO + \frac{1}{2}xH_2O \quad (1)$$

$$HCOOH_{(l)} \rightarrow H_{2(g)} + Co_{2(g)} \quad (2)$$

$$CoO_{(s)} + H_{2(g)} \rightarrow Co_{(s)} + H_2O_{(g)} \quad (3)$$

It showed that by increasing the temperature from 340 to 420 °C, 10 times more of CH_2O_2 was required to obtain completely metallic CoNPs, indicating that much more H_2 was needed. However, the required amount of H_2 was much less than the calculated one based on ideal gas law since H_2 fugacity was significantly improved around the critical point of water, so lower H_2 volume was needed. In another research, CoNPs were synthesized through one-step hydrothermal method using oleic acid as the capping agent. These NPs exhibited ferromagnetic behavior over a temperature range from 20 to 300 K [57].

Solvothermal method, which is similar to the hydrothermal technique with the exception of using an organic solvent instead of water [94], is also employed to create various Co nanostructures [58]. Liu et al. [58] mixed $C_4H_6CoO_4{\cdot}4H_2O$ with NaOH and dissolved the mixture in 1,2 propanediol under stirring and mild heating. Next, the mixture of sodium stearate ($C_{18}H_{35}NaO_2$) and hexachloroiridic acid hexahydrate (H_2-$IrCl_6{\cdot}6H_2O$) dissolved in 1,2-propanediol was added to the former mixture to create a flocculent solution. Then, the resultant solution was gradually heated to 150 °C in an autoclave. Finally, the precipitate was washed and dried under vacuum to obtain CoNPs. As shown in Fig. 1, the morphologies of CoNP depended on the Ir:Co ratio. In the absence of Ir, the spherical NPs were formed, and increasing the Ir:Co molar ratio to 0.01 resulted in nanorods. Further increasing the Ir:Co ratio to 0.025 and 0.050 had a negligible effect on the nanorod diameter but reduced their length from 100–300 nm to 50–200 nm and 40 nm, respectively. Chen et al. [59] illustrated that nucleation and growth of crystalline NPs can be governed by organometallic complexes through an intermediate agglomeration phase. This two-step solvothermal technique included a prenucleation step and a growth step. The prenucleation step was based on thermolysis of a calixarene complex with multiple Co_2-alkyne ligands (Co_{16}-calixarene 1) above 130 °C, creating coated cluster intermediates which agglomerated and formed Co nanoclusters. In the subsequent growth step, pentyne-$Co_4(CO)_{10}$ (PTC) monomers which have low thermal activation threshold were added to stop nucleation and promote crystalline growth.

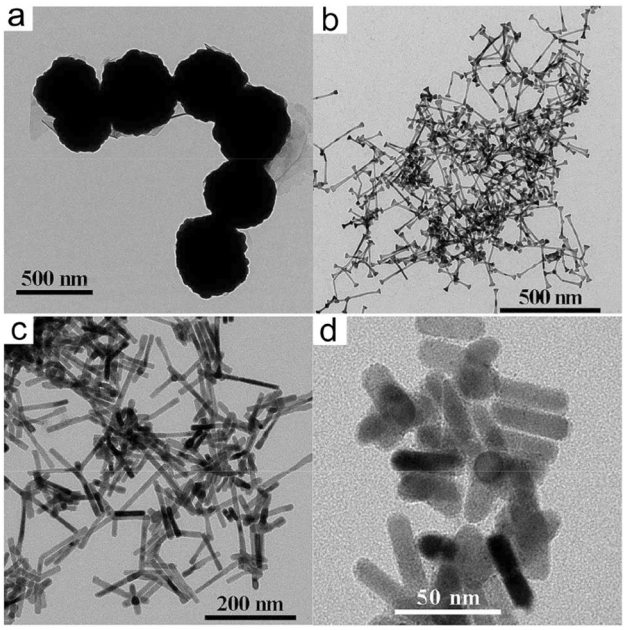

Fig. 1 Transmission electron microscopy (TEM) micrographs of cobalt nanostructures developed through various Ir:Co molar ratios at 150 °C: **a** 0, **b** 0.01, and **c** 0.025 for 20 h, and **d** 0.05 for 10 h. Reproduced with permission from Ref. [58] Copyright 2015 RSC

Thermal decomposition (thermolysis) is also used to synthesize MNPs in the presence of ligands in an organic solvent at high temperatures. Yang et al. [60] produced CoNPs through the thermal decomposition of dicobalt octacarbonyl ($Co_2(CO)_8$). First, dichlorobenzene was heated to 220 °C under nitrogen (N_2) and mixed with oleic acid and triphenylphosphine (TPP). Simultaneously, $Co_2(CO)_8$ was admixed with dry dichlorobenzene and heated to about 60 °C under N_2 flow. By adding the latter solution to the flask containing the former mixture, the $Co_2(CO)_8$ decomposed, resulting in both the formation of Co nuclei and the release of carbon monoxide (CO). After depleting the released gas, the remained black solution was refluxed at 185 °C for 20 min, and subsequently cooled down to ambient temperature to generate CoNPs. These CoNPs, dispersed in heptane for 90 days, showed high stability against oxidation. Bönnemann et al. [61] used toluene-dissolved triisobutylaluminium ($Al(C_8H_{17})_3$) and mixed it with the aqueous solution of $Co_2(CO)_8$, keeping the mixture stirring at 110 °C for 18 h under an Ar flow. As the solution color changed to dark brown and a black precipitate was formed, it was cooled down to 20 °C, accompanying the addition of more $Al(C_8H_{17})_3$ followed by temperature increasing to 110 °C for 3 h.

Another process to synthesize CoNPs utilized a mixture of anhydrous o-dichlorobenzene (DCB) and oleic acid (OA) (or amine such as hexadecylamine (HDA) or octadecylamine (ODA)). Such mixture was added to degassed tri-octylphosphine oxide (TOPO) in a three-neck flask and then heated to reflux temperature of ~ 182 °C [62]. Then $Co_2(CO)_8$ was injected to the flask followed by the decrease of temperature after a few hundred seconds, resulting in black ferrofluid. The results showed that injecting $Co_2(CO)_8$ into DCB in the presence of OA resulted in spherical CoNPs with a broad size distribution. The addition of TOPO changed the morphology of NPs to nanodisks (NDs) after 10 s of growth initiation, but these NDs were dissolved back as the growth process continued. In addition, by performing post-heating after the temperature drop caused by the injection, new CoNPs were formed. It is worth noting that replacing TOPO with amine, increased the yield of ND. Bao et al. [63] determined that surfactants could influence the CoNP growth mechanism. By employing the combination of OA and TOPO, CoNPs grew through the diffusional mechanism, resulting in single-crystalline NPs. By replacing TOPO with dioctylamine (DOA) in the abovementioned combination, the growth was dominated by the aggregation mechanism, producing multiple-grained NPs. Moreover, using TOPO alone resulted in an Ostwald ripening process. The resulting

CoNPs were used to make CoNPs-based NVM device with strong charge storage characteristics [64].

Thermolysis can also be employed to decompose a metal–surfactant complex in a secondary surfactant solution. Salavati-Niasari et al. [65] used a co-surfactant complex including [$Co(aceto)_2$] and oleylamine (at 140 °C). After adding it to triphenylphosphine (TPP) followed by a vigorous stirring at 250 °C under Ar atmosphere, the CoNPs were obtained by aging the solution at 240 °C for 1 h. Similarly, CoNPs were synthesized via thermal decomposition of acrylamide cobalt nitrate complex. The evaluation of magnetic properties of resulted CoNPs illustrated that the coercivity of the NPs was synthesis temperature dependent, meaning that high thermolysis temperature caused high coercivity of CoNPs [66]. The CoNCs synthesized by thermolysis of $Co_2(CO)_8$ contained both hexagonal close-packed (hcp) and primitive cubic (ε) structures and their saturation magnetization was also synthesis temperature dependent [67]. Zola et al. [68] synthesized CoNPs through three different methods to evaluate the effects of the processing parameters on the NP morphologies. Thermolysis of $Co_2(CO)_8$ resulted in spherical NPs with a narrow size distribution using a various precursor to surfactant ratios. In both chemical reduction and polyol techniques, the composition of the solution played a critical role. In the case of chemical reduction, the amount of reducing agent $NaBH_4$ affected the NPs noticeably while for polyol, adjusting the amount of TOPO and oleic acid transformed the irregular-shaped NPs to spherical ones.

In addition to solution synthesis techniques mentioned above, MNPs can be produced via an electrodeposition method with precise control over size and morphology by adjusting both composition and current density [95, 96]. Schiavi et al. [69] produced CoNPs on an aluminum foil sheet via electrodeposition technique. The experiments were conducted using an aqueous solution of $CoSO_4{\cdot}7H_2O$ with Na_2SO_4 and H_3BO_3 as the supporting electrolyte and buffer, respectively. Platinum wire, silver/silver chloride electrode (SSCE), and aluminum foils were used as the counter electrode, reference electrode, and working electrode, respectively. It showed that lowering values of passing charge not only reduced the average size of CoNPs, but also improved the uniformity of the NPs size distribution. However, varying the working electrode potential did not affect the size of CoNPs.

Flame spray pyrolysis (FSP) is a newly developed method for MNP synthesis in which the vapor phase of a metal precursor is injected into a hot reactor using a nebulizer [11]. In 2006, Grass et al. [70] synthesized highly stable face-centered-cubic (FCC) CoNPs by employing FSP. In their synthesis process, Co-carboxylate-based precursor was dispersed by the oxygen inside a spray nozzle and ignited using a mixed methane-oxygen flame. Synthesized CoNPs were covered with a thin layer of cobalt oxide which protected the CoNP core against further oxidation in air. Later, the resultant core–shell structure was modified by adding acetylene to the flame spray pyrolysis, resulting in the controlled deposition of the carbon layer on the CoNPs [71]. Further experiments illustrated that aryl-functionalization of the NPs surface increased the shell thickness, which reduced cobalt release rates and slowed down metal reduction rates [72].

Ultrasonic spray pyrolysis (USP) is another gas-phase synthesis technique to synthesize MNPs, in which ultrasound is employed to make metal droplets from the precursor solution which are delivered to a heated reactor via carrier gas [97]. Gürmen et al. [73] prepared Co powders by USP using aqueous solutions of $Co(NO_3)_2$ followed by thermolysis of generated aerosols in a hydrogen atmosphere. It showed that reducing $Co(NO_3)_2$ concentration from 0.08 to 0.04 $mol{\cdot}L^{-1}$, decreased the mean size of NPs from 596 to 480 nm. Later, Shatrova et al. [74] performed a two-step USP process to make CoNPs. First, Co_3O_4 nanostructured microspheres were synthesized by USP, which were subsequently reduced to metal cobalt in a hydrogen atmosphere. Magnetic property evaluation of the resultant CoNPs demonstrated that while the temperature during pyrolysis did not influence the coercive force and the saturation magnetization of NPs, the temperature during reduction drastically affected the magnetic properties, where increasing the reduction temperature from 220 to 350 °C decreased the coercive force (Hc) from 3.33×10^4 to 1.82×10^4 $A{\cdot}m^{-1}$.

Ion sputtering is a physical synthesis method in which a target material is vaporized through sputtering with a beam of inert gas ions at low pressures, followed by deposition of collimated NP beams on a substrate [98]. Chung et al. [75] fabricated CoNPs on SiO_2/Si (001) substrates through direct current (DC) magnetron sputtering at room temperature. Applying large positive biases limited the NPs growth and improved the uniformity of size distribution. Ion implantation is another physical approach in which ions are implanted into another solid material, changing its physiochemical properties [99]. Jacobsohn et al. [76] produced CoNPs through the implantation of 35 keV Co^+ ions into fused silica with various doses at room temperature. The results confirmed that a minimum Co concentration of about 2% was required to initiate the CoNPs precipitation. Furthermore, by increasing the implantation dose, the mean size of resultant CoNPs increased while the size distribution showed negligible change. In another study, CoNPs were produced through Li^{3+} and O^{7+} ions bombardment [77]. First, a 25-nm layer of Co was deposited on n-type silicon (100), and then it was cleaned by acetone- and methanol-sonication and subsequent e-beam evaporation. Finally, it was bombarded with 45-meV Li^{3+} and 100-meV O^{7+} ions. The atomic force microscopy (AFM) results showed that increasing in radiant exposure of ion increased the density

of CoNPs. Based on the consistent shape and height of Co peaks in the Rutherford backscattering spectroscopy (RBS) analysis, the absence of any sputtering, mixing, or diffusion of Co into the silicon matrix was confirmed, suggesting the film repositioned into a NP structure through a self-organized process.

Arc discharge is also used for the nanomaterial synthesis, in which a potential difference across two electrodes generates thermal plasma. El-Khatib et al. [78] synthesized CoNPs via a two-step arc discharge method in which cobalt precursor droplets were prepared using an ultrasonic nebulizer, and subsequently pyrolyzed by applying arc discharge between two silver electrodes in an Ar gas at atmospheric pressure. Jyothi et al. [79] synthesized CoNPs via laser ablation technique in which supersaturated Co vapor was produced by pulsed laser. The dipole moment of the surrounding environment was the main parameter affecting the growth, aggregation, and precipitation of CoNPs. Measurements of the optical properties of synthesized NPs demonstrated that by changing the solvent of CoNPs, the optical limiting threshold (decrease in the transmittance of the solution under high-intensity illumination) varied, where CoNPs dispersed in chlorobenzene and chloroform showed superior optical limiting comparing those NPs dissolved in other solvents such as benzene, carbon tetrachloride, toluene, and ethanol. These useful limiting characteristics of CoNPs resulted from significant two-photon and nonlinear scattering. Yılmaz et al. [80] employed a method named pulsed wire evaporation (PWE) to synthesize CoNPs while avoiding common contamination in chemical synthesis techniques. To do this, a high-power pulsed DC current as charging voltage passed through a Co wire to explode it, followed by subsequent evaporation and plasma formation. The as-formed plasma was cooled down by interacting with nitrogen gas, forming CoNPs. As shown in Fig. 2, the mean size of NPs was reduced by increasing the charging voltage. As the wire converted into the combination of vapor and droplets with sizes about the crystallite size of the initial wire, the crystallite size defined the CoNPs size. Accordingly, applying a charging voltage of 24 kV resulted in more polycrystalline NPs than the single crystalline ones in vapor-droplet mixture. By increasing charging voltage to 26 kV, the number of single-crystalline NPs increased, and applying 28 kV could generate purely single-crystalline NPs.

There are few studies using the biogenic method to synthesize CoNPs. In this technique, various microorganisms such as bacteria, fungi, actinomycetes, yeasts, viruses, and plant extracts and their enzymes are employed as reducing agents [100]. These techniques are cost effective, ecofriendly and require much milder synthesis conditions than those of many chemical and physical synthesis techniques [11]. Siada et al. [81] synthesized CoNPs using a mixture of 5 wt% of

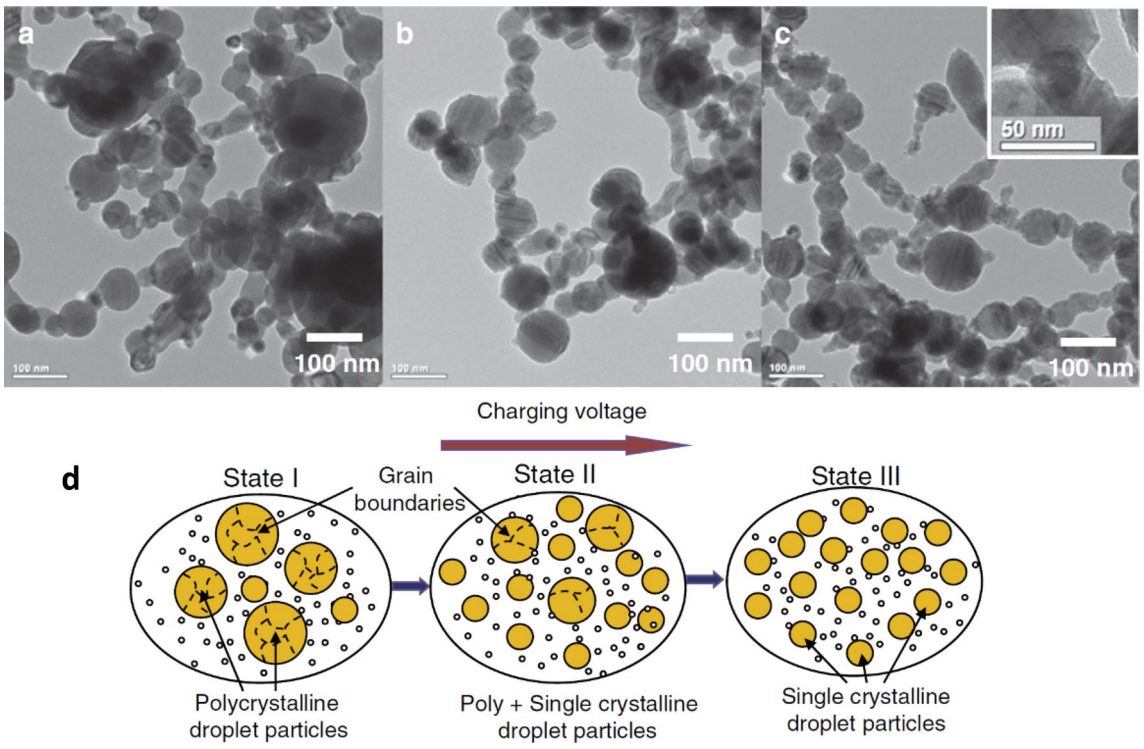

Fig. 2 TEM micrographs of CoNPs formed by various charging voltages of **a** 24 kV, **b** 26 kV, and **c** 28 kV. **d** Simple schematic of CoNP synthesis mechanism through PWE approach with different charging voltages. Reproduced with permission from Ref. [80] Copyright 2013 Elsevier

Piper longum and carbon paste, resulting in CoNP-modified carbon paste (CoNPsMCPE). Cyclic voltammetry and chronoamperometry results confirmed that the CoNPsMCPE exhibited good ascorbic acid oxidation activity in alkaline media, demonstrating its potential as an ascorbic acid sensor. Igwe et al. [82] used leaf extract of *Chromolaena odorata* (*C. Odorata*) to synthesize antibacterial CoNPs. These CoNPs inhibited the growth of several bacterial species, such as *E. coli*, *K. pneumonia*, *S. aureus*, and *S. pyogene*, showing their potential for use in disease treatment and control. Similarly, CoNPs synthesized with *Asparagus racemosus* root extract demonstrated notable antibacterial behavior against the human pathogenic bacteria *S. Dysenteriae* and *E. faecalis* compared to the common antibiotic Ciprofloxacin [44]. In another research, leaf extract of *Conocarpus erectus* and *Nerium indicum* of which phenolic compound levels were 296 ± 9 $\mu g \cdot g^{-1}$ and 185 ± 6 $\mu g \cdot g^{-1}$, respectively, were used. It showed that *Conocarpus erectus* possessed higher reducing power than that of *Nerium indicum* for CoNPs synthesis, suggesting that phenolic compounds act as reducing agents [83].

2.2 Cobalt-based nanocomposites

Yao et al. [42] employed hydrothermal approach to integrate Co on graphene oxide nanosheets (Co@GO NSs). An aqueous solution of $Co(NO_3)_2 \cdot 6H_2O$ was added to the uniform dispersion of GO, followed by adding ammonia to make the pH of ~ 10 and stirring for 4 h. Then, hydrazine hydrate was added to the solution, and the solution was heated up to 80 °C and then stirred for 5 h. Finally, the solution was cooled down and precipitate was collected and washed followed by annealing at 500 °C for 2 h under Ar/H_2 flow to form Co@GO hybrids. Due to the activation of graphene caused by peroxymonosulfate (PMS) and the dispersion of CoNPs as well, the resultant Co@GO NSs showed higher catalytic activity in the degradation of Orange II than that achieved by CoNPs without GO. Later, a liquid-phase plasma reduction method was used to integrate CoNPs on graphene sheets to create Co/graphene nanocomposites [84]. In another research, Gubin et al. [85, 86] integrated CoNPs into PE matrix through the thermolysis of cobalt formate ($C_2H_2CoO_4$) in hydrocarbon oil-melted PE at 200–260 °C under Ar, followed by cooling and washing. The resultant CoNPs exhibited rather high coercive force at room temperature, suggesting that they could serve as potential materials for magnetic recording applications.

Co@N-CNTs are considered efficient catalysts for ORR in fuel cells since CoNPs create centers with high activity toward ORR [101, 102]. Wang et al. [87] employed thermolysis to fabricate Co@N-CNTs catalysts. First, they mixed $Co(NO_3)_2 \cdot 6H_2O$ and melamine and adjusted the pH to about 2.5 by adding HCl solution. After drying, the resultant xerogel was carburized at 550 °C, followed by adding glucose as the reducing agent. This calcination process produced the pyridinic nitrogen and pyrrolic nitrogen, which were active sites for ORR. Finally, as the temperature increased to 900 °C for 3 h under Ar atmosphere, NTs formed. Adding glucose provided a sufficient source of carbon for pyrolysis, and prevented the formation of cobalt oxide. Another research group also produced Co@N-CNTs through a two-step pyrolysis process (see Fig. 3) [88]. Cobalt acetate tetrahydrate and Poly(ethylene glycol)-blockpoly(propylene glycol)-block poly(ethylene glycol) (P123) were dissolved in HCl, and then dicyanamide (DCDA) was added to it as the reducing agent, followed by drying the solution at 50 °C. Finally, two steps of pyrolysis were conducted at 400 °C and 900 °C under N_2 flow. Based on microstructure evaluation, it strongly suggested that the presence of Co facilitated the formation of CNTs and also increased the graphitization level of CNTs.

3 Metal palladium nanoparticles

PdNPs are among the most applicable and highly efficient catalysts to build C–C bonds and conduct other chemical transformations such as carbon-heteroatom bond formation, hydrogenation, carbonylation and oxidation processes [103–105]. They also showed promising potential for hydrogen generation and storage [106, 107]. Furthermore, they can be employed for other applications including chemical and biological sensors [108, 109], supercapacitors [110], and lithium-ion batteries [111, 112]. A list of methods used for PdNPs synthesis and their applications is presented in Table 2.

3.1 Pure palladium nanoparticles

Chemical reduction methods are widely used to produce PdNPs. Srimani et al. [113] synthesized PdNPs using a Fischer carbene complex of tungsten and polyethylene glycol (PEG) as the reductant and capping agent, respectively. These PdNPs, having high stability after 1 month, exhibited extensive catalytic activity in Hiyama cross-coupling reactions. The efficiency of reaction in water was much higher than that in co-solvents such as tetrahydrofuran (THF) or *N*,*N*-dimethyl formamide (DMF). Similarly, PdNPs with the large active surface area for electrochemical reactions were synthesized through the reduction of palladium(II) acetylacetonate ($Pd(acac)_2$) in oleylamine and borane tributylamine complex (BTB) [114]. In this process, oleylamine acted as the solvent, surfactant, and reductant while BTB served as a co-reductant. Vancová et al. [115] produced PdNPs by reduction of $PdCl_2$ with sodium citrate and mixing

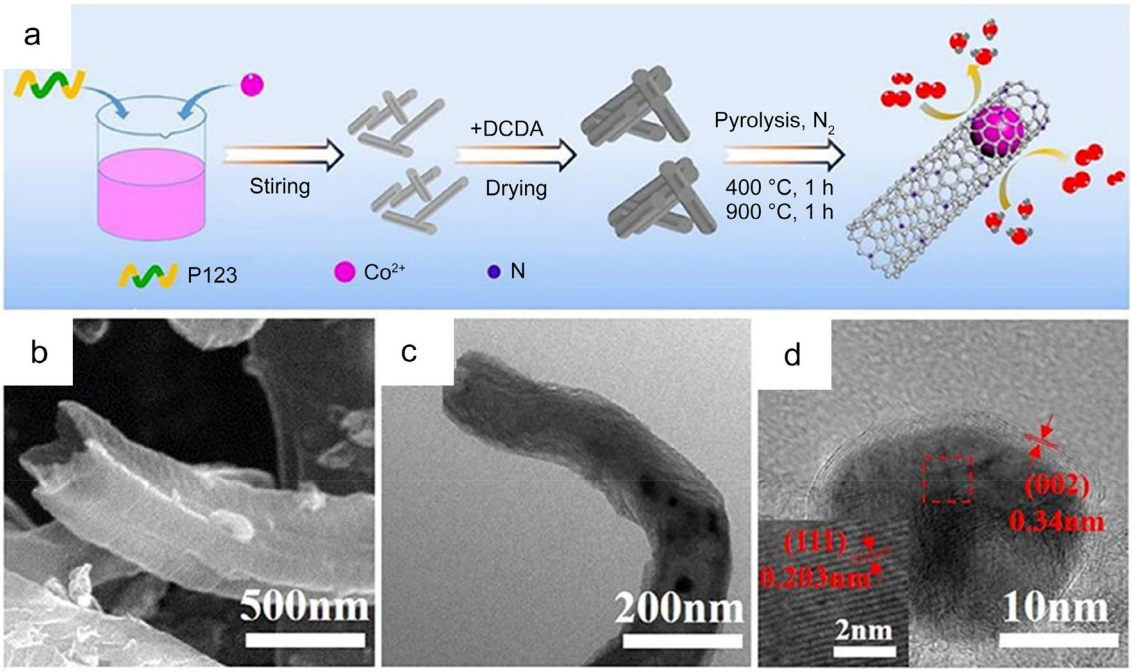

Fig. 3 **a** Simple presentation of synthesis steps of Co@NC NTs. **b** Field emission scanning electron microscopy (FESEM), **c** TEM, and **d** high-resolution TEM (HRTEM) microstructure images of the Co@NC NTs [88]

with Dihydrolipoic acid (DHLA). The resulting NPs were conjugated successfully to the protein molecules such as streptavidin, protein A, or avidin via the cross-linking agent 1-ethyl-3-(3-dimethylaminopropyl)carbodiimide (EDC).

Developing Pd nanostructures is not limited to NPs and is expanded to synthesize nanostructures with different morphologies. Huang et al. [116] synthesized Pd nanowires (PdNWs) and Pd nanorods (PdNRs) by hydrothermal reduction of palladium(II) chloride with polyvinylpyrrolidone (PVP) as both surfactant and reductant in the presence of sodium iodide (NaI) at 200 °C. NaI played a critical role in this process since without the I^- ions, and some PdNPs were formed among the PdNWs network. As shown in Fig. 4, by increasing the reaction time from 1.5 to 8 h, the aspect ratio of Pd nanostructures reduced from about 220 to 6, indicating the transformation of PdNWs to PdNRs.

Sonochemical technique is another chemical synthesis method in which exposure of liquids to ultrasound creates acoustic waves that form bubbles and fluctuates them. As the bubbles overgrow they collapse and release concentrated energy, meaning that each cavitation bubble performs as a plasma chemical microreactor and develops a highly energetic environment at almost room temperature [11, 155]. Nemamcha et al. [117] synthesized PdNPs using a sonochemical process. An aqueous solution of $Pd(NO_3)_2$ was added to the mixture of ethylene glycol (EG) and PVP, and then the resultant solution was irradiated with ultrasonic waves for 180 min. Microstructure examination confirmed that by increasing the Pd(II)/PVP molar ratio, the number of PdNPs decreased and their size increased from 3 to 6 nm. Further research confirmed that as the current density increased from 8 to 13 $mA{\cdot}cm^{-2}$, the average size of PdNPs decreased from 20 to 5 nm [118]. Moreover, changing the deposition time between two continuous sonic pulses from 1 to 5–10 s increased the number of PdNPs and narrowed their size distribution. The concentration of cetyltrimethylammonium bromide (CTAB) (as the reductant) influenced the NP growth, where the concentration below 5 $mmol{\cdot}L^{-1}$ resulted in aggregated irregular-shaped NPs, but with the concentration more than 50 $mmol{\cdot}L^{-1}$ well-dispersed spherical NPs were created. By continuing the reaction for more than 2.5 h, dendritic nanostructures were obtained due to the accumulation and growth of PdNPs at the anode.

Recently, polyol techniques have emerged as suitable soft chemical methods to produce MNPs. In addition to the interesting reducing ability of polyalcohols or polyols, they exhibit several desirable characteristics for MNP synthesis including high boiling points allowing high-temperature syntheses, protecting as-prepared materials against oxidation, ability to coordinate metal precursor preventing aggregation, and high viscosity, resulting in the controlled structure and morphologies [156]. Li et al. [119] synthesized Pd icosahedra by preparing an EG solution containing sodium tetrachloropalladate (Na_2PdCl_4) and PVP, stirred and heated in air at 120 °C for 48 h. TEM micrographs of PdNPs in Fig. 5 shows the high density of twin boundaries, which,

Table 2 Different synthesis methods of PdNPs

NP type	Synthesis method	Function	Size (nm)	Shape	References
PdNPs	Chemical reduction	Catalyst for Hiyama cross-coupling reactions	9.70	Sphere	[113]
PdNPs	Chemical reduction	Catalyst for formic acid oxidation in $HClO_4$ solution	4.5	Sphere	[114]
Protein-PdNPs	Chemical reduction	Labeling in electron microscopy	10	Sphere	[115]
PdNRs and PdNWs	Hydrothermal	–	5–19 (diameter)	Rod	[116]
PdNPs	Sonochemical	–	3–6	Sphere	[117]
PdNPs	Sonochemical	Potential catalysis applications	4–5	Sphere and dendrite	[118]
PdNPs	Polyol	Catalyst for low-temperature reduction of automobile pollutants, hydrogenation reactions, and hydrogen storage	15–42	Icosahedron	[119]
PdNPs	Polyol	Catalyst for hydrogenation of alkenes, alkynes, nitro derivatives, benzaldehydes, aromatic ketones	1.4–1.7	Sphere	[120]
PdNRs	Seed-mediated growth	Catalysts for Suzuki reactions	200 and 300 (diameter)	Rod	[121]
PdNCs	Seed-mediated growth	Potential applications in SERS	22	Cube	[122]
PdNCs, PdPNCs, PdNRDs, and BPdNCs	Seed-mediated growth	Catalysts for hydrogenation/dehydrogenation reactions	10–20	Cube, protruded cube, and rhombic- dodecahedron	[123, 124]
HPdNCs	Seed-etching	–	10	Cube	[125]
PdNPs	Biogenic	Recovering platinum group metals form wastewater	50	Sphere	[126]
PdNPs	Biogenic	–	<30	Sphere	[127]
PdNPs	Biogenic	Catalysts for Suzuki reaction	4–16	Sphere	[128, 129]
PdNPs	Biogenic	–	20–60	Sphere	[130]
PdNPs	Biogenic	Catalyst for Suzuki reaction	96.4	Sphere	[131]
PdNPs	Biogenic	Catalysts for aromatic alcohol oxidation	2.2	Sphere	[132]
PdNPs	Biogenic	Potential catalyst and antimicrobial agent	2–4	Sphere	[133]
PdNPs			60–70		
Pd-LA NPs	Biogenic	–	65–80	Sphere	[134]
Pd-Vitamin-LA NPs			75–100		
PdNPs	Biogenic	Catalyst for Mizoroki–Heck cross-coupling reaction	2–15	Sphere	[135]
PdNPs	Biogenic	Potential catalysis in the degradation of azo dyes	15	Sphere	[136]

Table 2 (continued)

NP type	Synthesis method	Function	Size (nm)	Shape	References
PdNPs	Biogenic	Antibacterial against *E. coli* catalyst for reduction of 4-NP	4–9	Sphere	[137]
PdNPs	Biogenic	Catalytic properties in degradation reaction of azo dyes	2.5	Sphere	[138]
PdNPs	Biogenic (continuous microreactor)	Catalyst for the reduction of 4-NP	4.40 ± 1.68	Cube	[139]
	Biogenic (batch)		7.18 ± 21.14		
Pd@HHSS hybrids	Chemical reduction	Catalytic activity in Suzuki reaction	5–10	Sphere	[140]
Pd@CNF hybrids	Chemical reduction	Catalyst for electrooxidation of liquid fuels	4.2	Sphere	[141]
Pd/Fe_3O_4, Pd/Co_3O_4, and Pd/$Ni(OH)_2$	Microwave irradiation-assisted reduction	Potential catalyst for oxidation of CO	6–8	Sphere	[142]
Pd@Graphene nanocomposites	Hydrothermal	Efficient catalyst for the Suzuki reaction	4 and 15	Sphere	[143]
Pd-Graphene and Pd-Carbon hybrids	Electrodeposition	Catalyst for ORR of direct methanol fuel cells	73–1000	Sphere	[144]
Pd@Graphene nanocomposites	Wet impregnation	Hydrogen sensor applications	10	Sphere	[145]
Pd@RGO nanocomposites	Pulsed laser ablation	Catalytic activity for CO oxidation	5–12	Sphere	[146]
Pd@Al_2O_3 nanocomposites	Microwave plasma torch	Potential catalyst for isomerization of 1-butene	10–50	Sphere	[147]
Pd@SiO_2 nanocomposites	Sonochemical	–	5–6	Sphere	[148]
Pd-RGO-CNT composites	Combined hydrothermal and redox	Catalyst for reduction of 4-NP	4	Sphere	[149]
Pd-Cu bimetallic NPs	Polyol	Catalysts for semi-hydrogenation of alkynes and azide-alkyne cycloaddition	3–4	Sphere	[150]
Pd-Ru bimetallic NPs	Polyol	–	3–10	Sphere	[151]
Pt–Pd bimetallic NPs	Microwave-assisted polyol	–	6.2	Sphere	[152]
Hollow Ag-Pd bimetallic NPs	Galvanic replacement and coreduction	Catalyst for reduction of 4-NP	14.6 ± 2.0	Sphere	[153]
Pd@Lignin nanocomposites	Mechanochemical milling	–	3.2 (Palladium(II) chloride)	Undefined	[154]
			2.8 (Palladium(II) acetate)	Sphere	
			3.6 (Palladium(II) acetylacetonate)	Sphere	

PdNCs palladium nanocubes, *PdNRs* palladium nanrods, *PdNWs* palladium nanowires, *CNF* carbon nanofiber, *RGO* reduced graphene oxide, *PdNRDs* palladium nano rhombic dodecahedra, *PdPNCs* palladium protruded nanocubes, *BPdNCs* branched pappadium nanocubes, *CNT* carbon nanotube, *HHSS* hollow silica sphere, *SERS* surface-enhanced Raman scattering, *LA* lipoic acid

combined with the sharp edges of icosahedral PdNPs, result in high catalytic activity. In yet another study, a mixture of $PdCl_2$(cod) and choline-based derivative such as choline chloride or choline *N*-tosylalaninate were dissolved in glycerol and stirred under Ar at 80 °C for 18 h, which resulted in the formation of PdNPs. These PdNPs were well-dispersed because the supramolecular structure of glycerol effectively prevents the agglomeration of NPs [120].

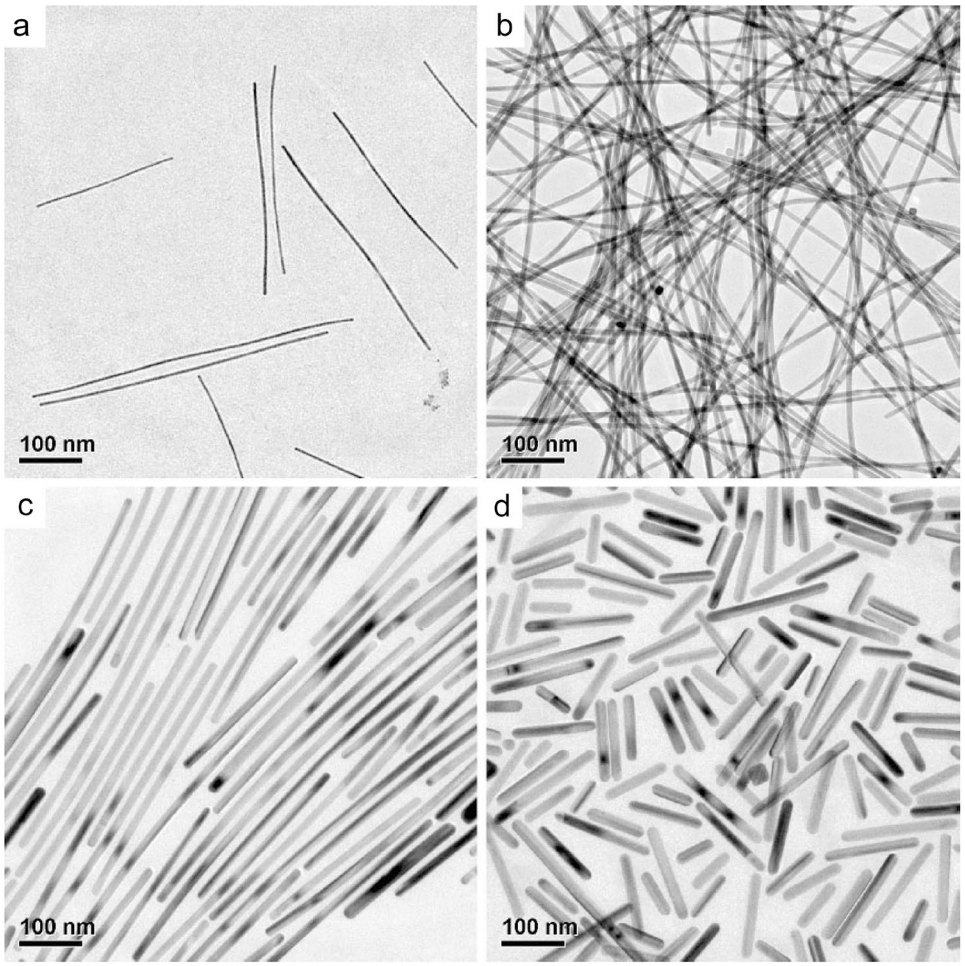

Fig. 4 TEM micrographs of the one-dimensional Pd nanostructures produced in **a** 1.5, **b** 2.0, **c** 4.0, and **d** 8.0 h of reaction time. Reproduced with permission from Ref. [116] Copyright 2009 American Chemical Society

Pd nanostructures are also synthesized using a seed-mediated technique [121]. To produce Pd nanoseeds, $PdCl_2$ and NaCl were dissolved in deionized water to make H_2PdCl_4 solution, and the solution was bubbled with Ag to prevent re-oxidation. Then this solution was injected to a two-neck flask containing CTAB (the surfactant). Next, $NaBH_4$ aqueous solution was added into the mixture under N_2 flow. To synthesize PdNRs, two vials were tagged A and B. The growth solution was made in both vials by mixing CTAB with H_2PdCl_4. Ascorbic acid was added to vial A as the reducing agent, and Pd nanoseeds were also added to vial A and kept for 2 h to form a blackish green solution. Then, copper(II) acetate ($Cu(OAc)_2$) solution was added to vial B, followed by the addition of ascorbic acid. Part of vial A was transferred to vial B and the mixture was left at 30 °C for 20 h to precipitate PdNRs. As it is shown in Fig. 6, by increasing the amount of $Cu(OAc)_2$ solution, the faceted NPs turned into the branched nanostructures, while short rods transformed to longer rods with branches developed at the two ends.

In another set of experiments, the same approach was employed to make Pd nanocrystals with different shapes, as seen in Fig. 7 [122–124]. To make the cube-shape seeds, the mixture of CTAB solution was heated at 95 °C followed by the addition of H_2PdCl_4 solution. Next, ascorbic acid was admixed and stirred for 10 min, and subsequently cooled down to 30 °C and left aging for 1 h. To grow Pd nanocubes (PdNCs), a solution including CTAB in deionized water was mixed with H_2PdCl_4 and stirred in a water bath at 45 °C. Next, Pd cube-shaped seeds were added to the solution followed by the addition of ascorbic acid and stirring at 45 °C for 6 h to precipitate PdNCs. Pd nano rhombic dodecahedra (PdNRDs) were made by adding NaI to the CTAB solution prior to the addition of H_2PdCl_4. Also, replacing NaI with Cu_2SO_4 induced the formation of Pd protruded NCs (PdPNCs). To make the branched PdNCs (BPdNCs), the polygonal seeds (instead of cubic seeds) were prepared via the same method except the addition of $NaBH_4$ aqueous solution into the mixture of CTAB and Na_2PdCl_4. In addition, through the growth step, the Cu_2SO_4 solution was added to the CTAB solution before the addition of Na_2PdCl_4 [124].

Successful synthesis of Pd nanostructures with various shapes inspired scientists to utilize seed-based approaches to design more complex-shaped PdNPs. Wei et al. [125]

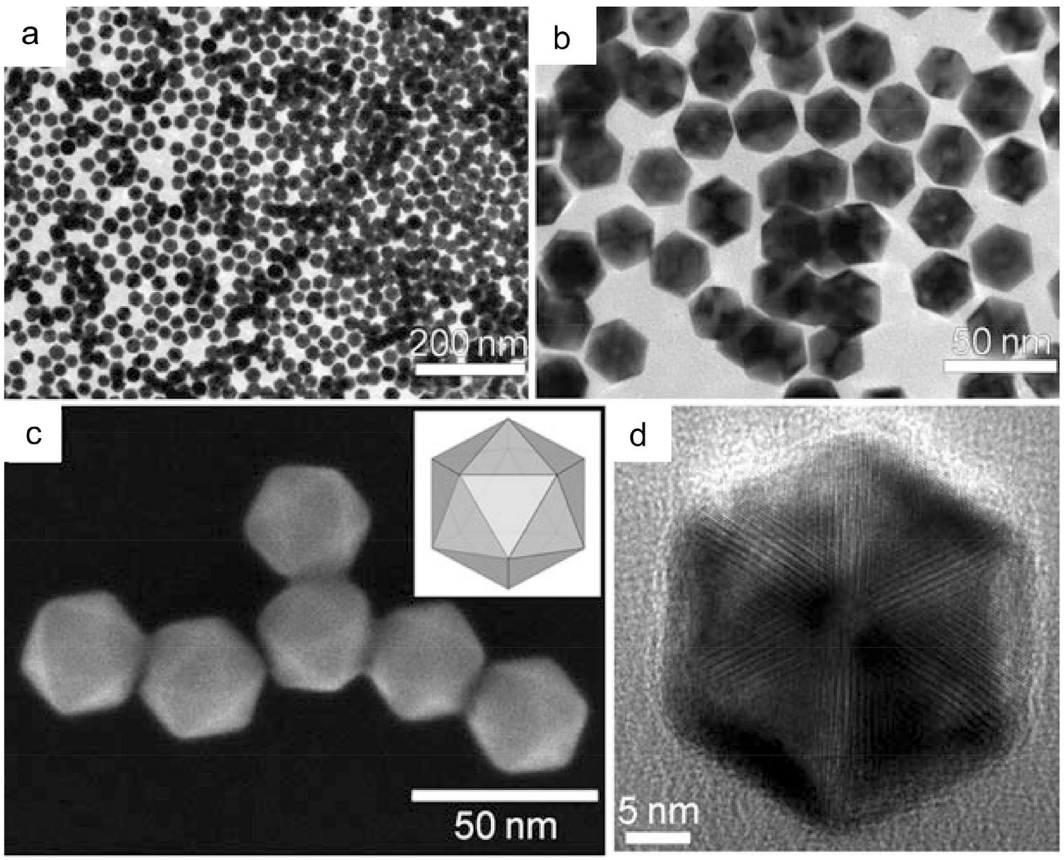

Fig. 5 **a** Low and **b** high magnification TEM images and **c** FESEM image of the icosahedral PdNPs. **d** HRTEM image of a single Pd icosahedron. Reproduced with permission from Ref. [119] Copyright 2009 John Wiley and Sons

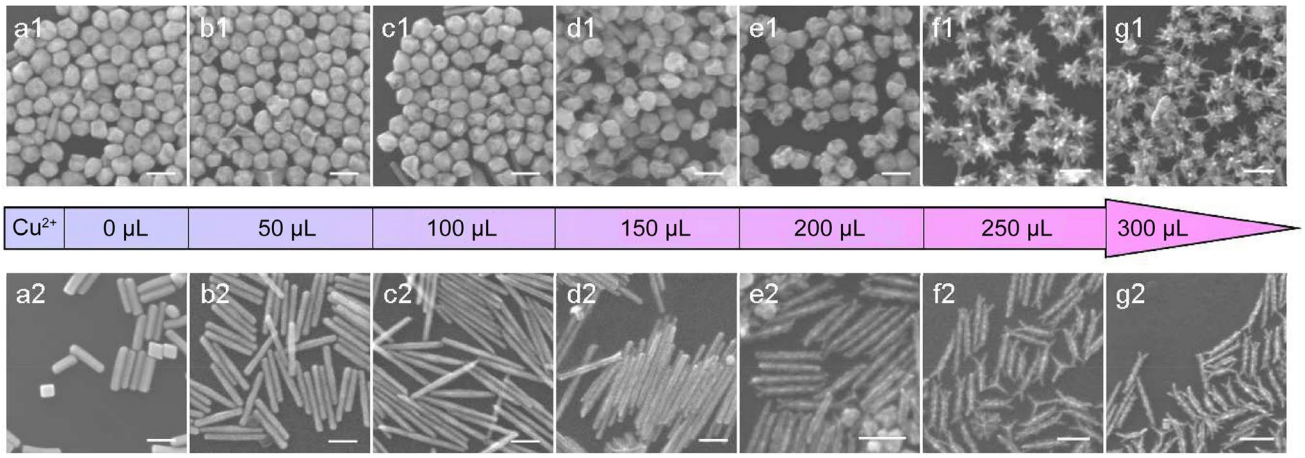

Fig. 6 SEM images of the Pd nanostructure developed through adding different volumes of the $Cu(OAc)_2$ solution. Reproduced with permission from Ref. [121] Copyright 2009 American Chemical Society

synthesized hollow Pd nanocages (HPdNCs) through the seed-etching approach. To make the initial PdNCs, sodium tetrachloropalladate(II) (Na_2PdCl_4), sodium hydroxide (NaOH), and CTAB were dissolved together in deionized water and stirred vigorously at 95 °C, and then ascorbic acid was added into the solution and the reaction was kept running for 30 min. Afterwards, the resultant PdNC seeds were dispersed in a chamber with reverse micelle. By heating, the

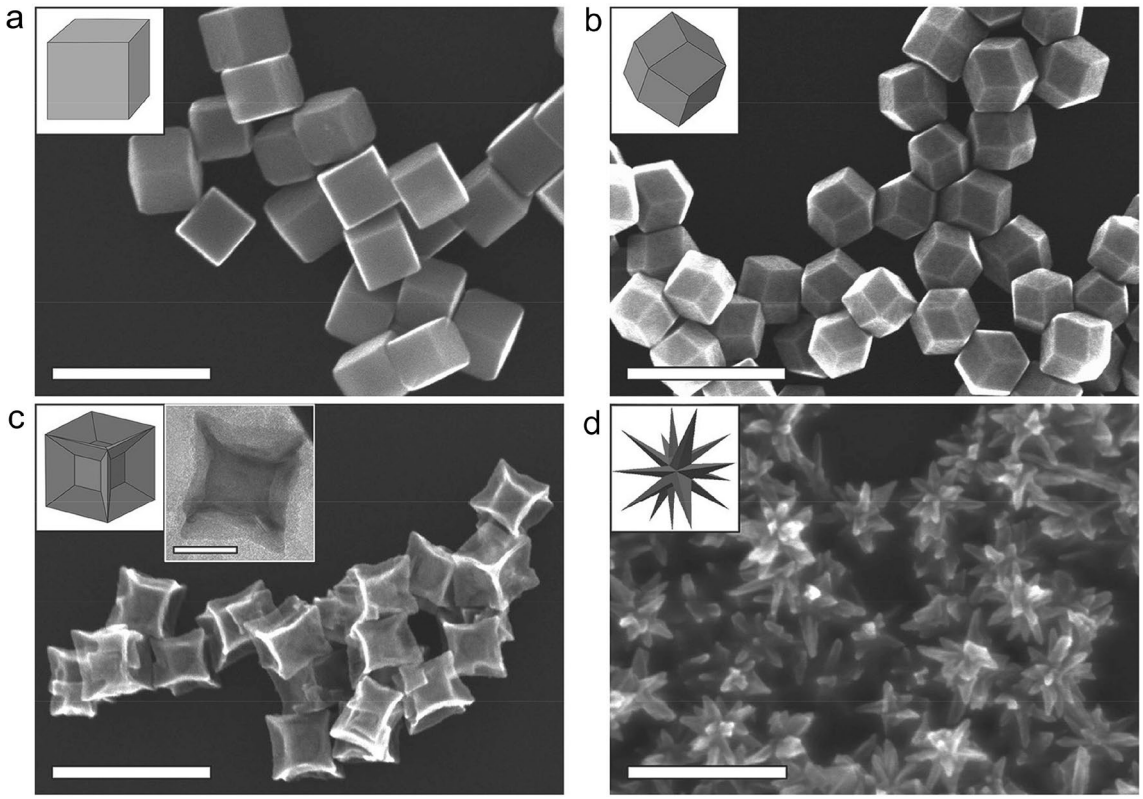

Fig. 7 SEM images of **a** PdNCs, **b** PdNRDs, **c** PdPNCs, and **d** BPdNPs (All scale bars are 200 nm). Also, a TEM image of PdPNCs with the scale bar of 50 nm is demonstrated in **c**. Reproduced with permission from Ref. [124] Copyright 2016 John Wiley and Sons

aqueous phase gradually evaporated, and subsequently the capping structure was disrupted by the diffusion of CTAB. As shown in Fig. 8, the decrease in the capping agents at the center of {200} plane is more noticeable than the edges, resulting in the desorption of Pd atoms from those sites, and leading to the formation of tube-shaped seeds.

The biosynthesis of PdNPs using bacteria [126, 127], viruses [128, 129], and plants [130–134] are also reported. SwaminathanáIyer et al. [135] synthesized PdNPs through photoautotrophic microalgal metabolism *of Chlorella vulgaris* which served as reducing agents. PdNPs were then incorporated on an electrospun chitosan mat as a novel support for applications in catalysis (see Fig. 9). Photosynthetic processes in green microalgae can take place either under oxygenic or anoxic environments. Green algae have chlorophyll-a and chlorophyll-b pigments and can accomplish oxygenic photoautotrophic reactions while using H_2O as an electron donor [157]. Oxygenic photoautotrophic processes contain light and dark photochemical reactions, in which light reactions conserve chemical energy in the form of adenosine triphosphate (ATP) and the reduced form of nicotinamide adenine dinucleotide phosphate (NADPH), and dark reactions cause reducing CO_2 to organic compounds using ATP and NADPH. CO_2 is fixed by the enzyme of ribulose bisphosphate carboxylase (RuBisCO) and reduced in the Calvin cycle using NADPH. Reducing equivalents can be exported from the chloroplast in the form of carbon metabolites, particularly triose phosphates (triose-P). Their oxidation by dehydrogenases in the cytosol can also generate nicotinamide adenine dinucleotide (NADH) and nicotinamide adenine dinucleotide phosphate (NADPH), which can be used as the reducing agent promoting the reduction of Pd(II) into PdNPs. Using another biogenic process, Petla et al. [136] synthesized PdNPs using *Glycine max* (*soybean*) leaf extract. The Fourier transform-infrared spectroscopy (FTIR) results suggested that the proteins and some of the amino acids existing in *soybean leaf* extracts were responsible for reducing the Pd ions.

Ullah et al. [137] used $PdCl_2$ as the precursor and glucosamine as the reductant and stabilizer to synthesize PdNPs. Based on the antibacterial activity, such PdNPs demonstrated higher activity against *E. coli* than tobramycin. This was attributed to the PdNPs' superior penetration of peptidoglycan, a vital component of the *E. coli* cell wall. The ions release from the penetrating PdNPs in the bacteria's cytoplasm and generate reactive oxygen species (ROS), inhibiting the bacteria growth via membrane damage and nucleic acid-protein inactivation. Similarly, carboxymethyl

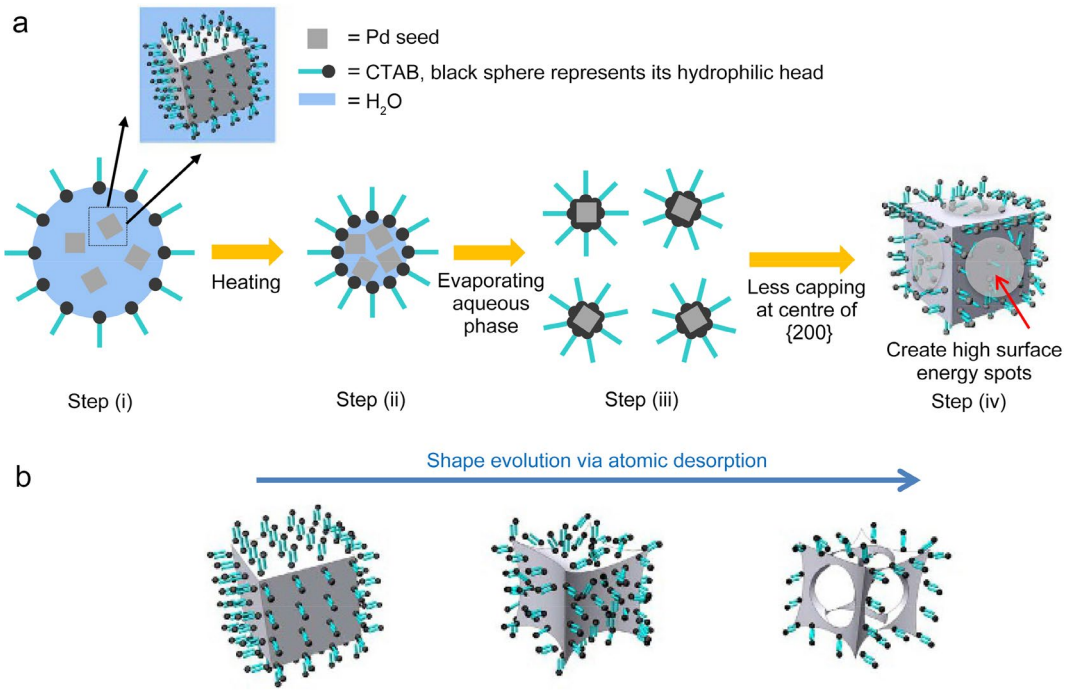

Fig. 8 **a** Different steps of shape evolution from PdNCs to HPdNCs via the seed-mediated etching, and **b** the etching of PdNCs at the center of {200} planes in the step (iv). Reproduced with permission from Ref. [125] Copyright 2014 Springer-Nature

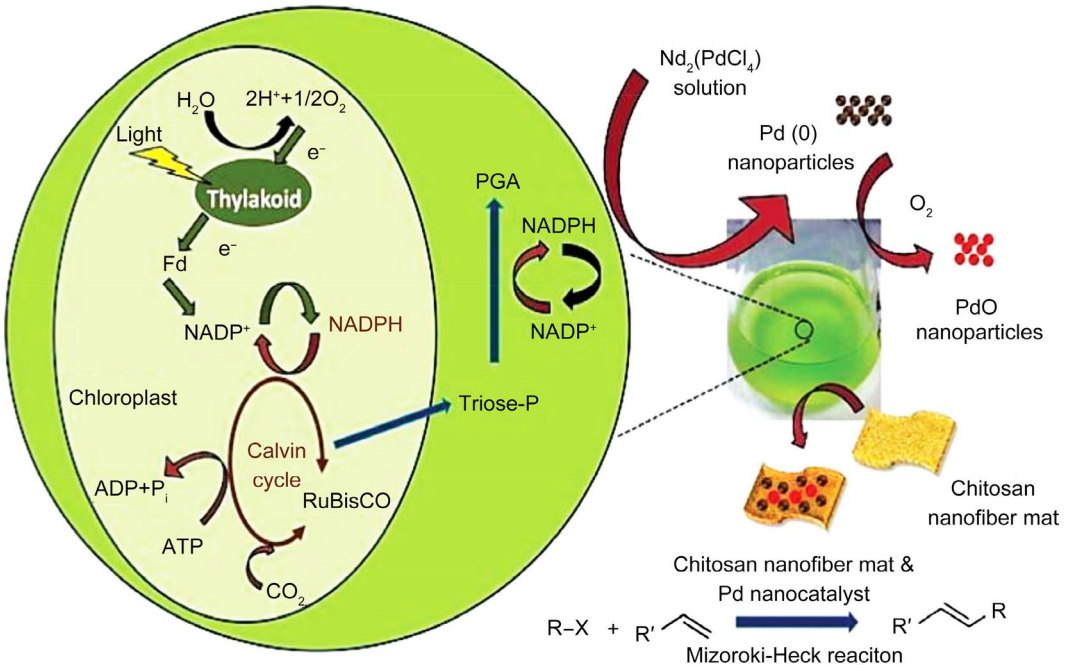

Fig. 9 Schematic of PdNP synthesis through photosynthetic microalgae and their application as a catalyst in Mizoroki–Heck reactions. Reproduced with permission from Ref. [135] Copyright 2013 Elsevier

cellulose (CMC) can act as both the stabilizer and reductant for green production of PdNPs [138]. Gioria et al. [139] compared the green synthesis of PdNPs using conventional batch and continuous microreactor approaches. For batch synthesis, NaOH was added to a mixture of H_2PdCl_4 and starch with pH adjusted to 5.5 and the reduction process

was conducted at 60 °C for 10 min. In continuous reaction, the NaOH aqueous solution and the aqueous mixture of $PdCl_2$–glucose-starch were loaded into two syringes, and consequently, pumped into the micromixer at 60 °C. The continuous technique resulted in uniformly distributed fine PdNPs which demonstrated higher catalytic activity in the degradation of 4-nitrophenol (4-NP) due to the higher surface area of smaller NPs.

3.2 Palladium-based nanocomposites

Chemical reduction approaches are also used to produce PdNPs with/on different supports, mainly for catalytic applications. Pd/SiO_2 nanohybrids were made using this approach [140]. First, HHSSs were prepared by dissolving CTAB in a mixture of H_2O and ammonia and subsequently adding n-octane to that emulsion. Then, tetraethyl orthosilicate (TEOS) was added to it, heated to 373 K, and kept for 24 h. Finally, the synthesized solid sample was collected and calcined at 550 °C for 6 h in air to remove CTAB and other organic components. To make Pd@HHSS nanocomposites, the resultant HHSSs were mixed with $Pb(OAc)_2$ with different ratios, and subsequently, a solution of $NaBH_4$ in EtOH was added. After 3 h stirring and subsequent washing with EtOH, it was heated to 70 °C and kept overnight. Through the impregnation step, palladium acetate $Pd(OAc)_2$ was transformed to Pd(II) oxide species at the surface of the HHSSs. After adding $NaBH_4$ as the reducing agent, PdNPs formed on the surface of HHSSs. Similarly, Ko et al. [141] employed sodium dodecyl sulfate (SDS) as the surfactant and $NaBH_4$ as the reductant to integrate PdNPs on CNF supports.

Elazab et al. [142] prepared PdNPs catalysts supported on Fe_3O_4, Co_3O_4, or $Ni(OH)_2$ nanoplates through mixing $Fe(NO_3)_3{\cdot}9H_2O$, $Co(NO_3)_2{\cdot}6H_2O$, or $Ni(NO_3)_2{\cdot}6H_2O$ with aqueous $Pd(NO_3)_2$ and hydrazine hydrate and subsequent microwaving in 60-s cycles for a total reaction time of 5, 7, and 9 min, respectively. Employing microwave irradiation promoted the reaction without requiring high temperature. Though T_{100} (the temperature at which the catalytic reaction is completed) of CO catalytic oxidation using $Pd/(NiO)_2$ as catalysts was almost the same as unsupported PdNPs, indicating weak interaction between PdNPs and the $Ni(OH)_2$ support, both the Pd/Fe_3O_4 and Pd/Co_3O_4 catalysts showed high activity. At about 127 °C, the percentage of CO conversion performed using Pd/Co_3O_4 and Pd/Fe_3O_4 as catalysts was 50 wt% and 30 wt%, respectively, suggesting strong interaction of PdNPs with Co_3O_4 nanoplates. In another research, Li et al. [143] used the hydrothermal approach to make graphite oxide (GO)-Pd hybrids. In this process, GO was first heated in NaOH solution followed by the addition of SDS aqueous solution. Then, $Pd(OAc)_2$ was added to the solution, followed by refluxing at 110 °C for 4 h. SDS acted as both a reducing agent and surfactant. Using 0.1 mol/L and 0.05 mol/L of SDS NPs with the mean size of 4 nm and 15 nm were produced, respectively, demonstrating the importance of SDS in the size control of (GO)-Pd hybrids. Similarly, microstructure evaluation of PdNPs electrodeposited on the graphene and carbon supports illustrated that with the increase of the SDS concentration from 0 to 14 m $mol{\cdot}L^{-1}$, the average size of PdNPs was reduced from about 1000 to 70 nm [144].

In another attempt to produce Pd@graphene nanocomposites, Tang et al. [145] impregnated the graphene support into $Pd(bipyridine)(pyrene)_2$ for 10 min to connect the Pd precursor molecules with the graphene support through π–π bonds. After washing, the sample was annealed at 300 °C for 40 min under H_2/Ar flow. The resulted nanocomposites were explored as a sensor for H_2. It showed that these sensors, which were adaptable with complementary metal–oxide-semiconductor (CMOS) circuits, were not affected by certain redox gases such as formaldehyde and ammonia. Moussa et al. [146] developed Pd-based nanocomposites by integrating PdNPs on RGO supports through one step laser irradiation of the mixture of GO aqueous solution and Pd nitrate. The synthesized nanocomposits showed excellent catalytic activity for CO oxidation. In another research, alumina (Al_2O_3)-supported PdNPs catalysts were synthesized via a microwave plasma torch method in which an aerosol including 0.5 wt% of $PdCl_2$ and 99.5 wt% Al_2O_3 were added into an atmosphere pressure plasma created by the microwave torch [147]. In addition, Chen et al. [148] synthesized SiO_2/Pd nanocomposites through ultrasound irradiation of mesoporous silica substrate, $PdCl_2$, and isopropanol at room temperature under Ar flow.

Sun et al. [149] developed a new type of catalyst by coating PdNPs on RGO-CNTs through a combined hydrothermal and redox approach. First, they used Hummer technique to make GO which contains many oxygen-containing functional groups, allowing GO to distribute uniformly in an aqueous solution. The amphiphilic characteristic of GO sheets makes them good surfactant. Hence, CNTs can be distributed into individual ones by ultrasonication and can form π–π bonds on the GO surface. By conducting hydrothermal processing on the mixture of the GO and CNT aqueous dispersion, macroscopic RGO-CNT cylinder hydrogels were formed, including well defined and interconnected three-dimensional (3D) porous network, and the pore walls were made of thin layers of accumulated RGO sheets (see Fig. 10). Finally, the Pd-RGO-CNT composites were formed through a redox reaction between the RGO-CNT composites and a K_2PdCl_4 aqueous solution in an ice bath, where the transport of the Pd^{2+} ions and electrons as well as anchoring of Pd precursors and the subsequent Pd nucleation took place throughout the 3D nanostructure of RGO-CNTs. The

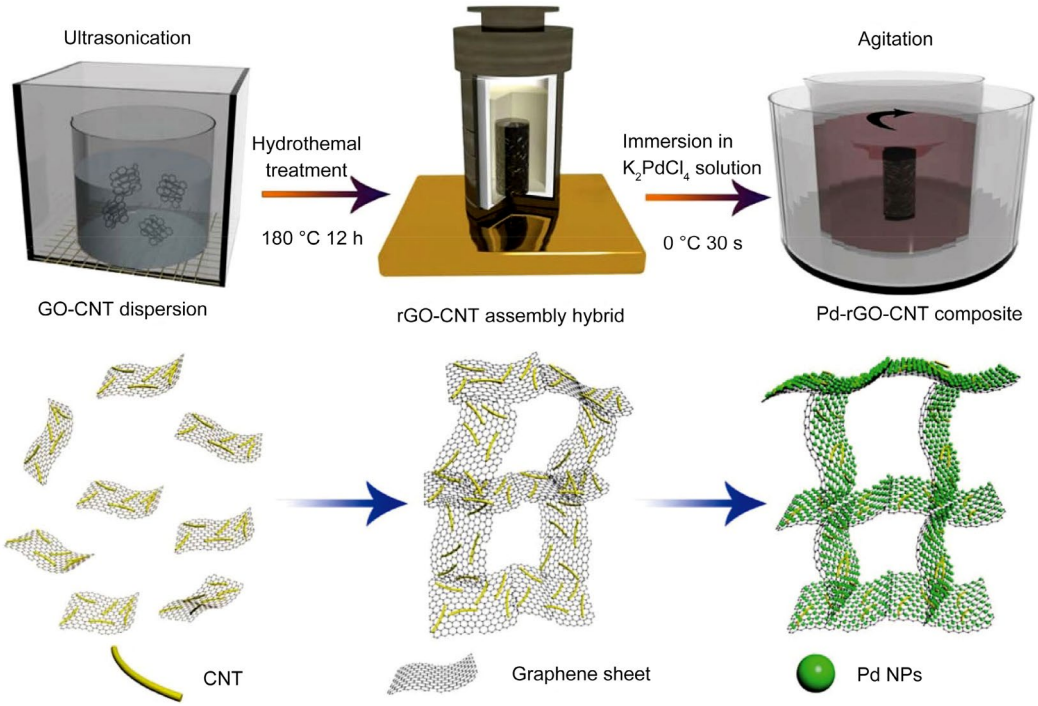

Fig. 10 Simple schematic of various synthesis steps of the Pd-rGO-CNT composites. Reproduced with permission from Ref. [149] Copyright 2013 Springer Nature

resultant nanocomposites (1.12 wt% Pd) were tested as a catalyst for reducing 4-NP to 4-aminophenol (4-AP) by $NaBH_4$. It showed that the reaction could complete in just 20 s at room temperature.

Dang-Bao et al. [150] employed polyol technique to synthesize Pd-Cu bimetallic NPs by co-reducing palladium acetate and $[Cu(TMEDA)(\mu\text{-}OH)]_2Cl_2$ (TMEDA: tetramethylethylenediamine) in the presence of glycerol and PVP at 120 °C. Changing the ratio of Pd:Cu ions varied the final microstructure. The Pd:Cu ionic ratio of 1:1, 1:2, and 2:1 resulted in Cu-coated PdNPs, disordered alloy, and monometallic samples, respectively. Similarly, Pd-Ru bimetallic NPs were synthesized by mixing $RuCl_3$ and K_2PdCl_4 precursors, adding the reductant solution containing PVP on a monomer basis in triethylene glycol (TEG), and heating the solution at 200 °C in a microflow reactor [151]. Cong et al. [152] synthesized Pt–Pd bimetallic NPs through a microwave-assisted polyol technique, in which the mixture of metallic ions and PVP were loaded in a single-mode 300 W microwave apparatus, and then heated to 471 K in EG for about 2–3 min. The same process could be applied in a continuous-flow reactor system for large-scale production.

Wu et al. [153] combined galvanic replacement and co-reduction reactions in a continuous series of coiled flow inverter (CFI) microreactors to produce hollow Ag-Pd bimetallic NPs. As shown in Fig. 11, by mixing sodium borohydride, sodium citrate, and silver nitrate in reactor 1, silver seeds were formed. Then, they were transferred to reactor 2 with the fresh mixture of $AgNO_3$ and trisodium citrate dihydrate (Na_3CA) to grow the Ag seeds. Finally, the resulting AgNPs were transferred to reactor 3 and mixed with $Pd(NO_3)_2$ solution and hydroquinone (HQ) that serves as a mild reducing agent.

Rak et al. [154] assessed the effect of the Pd precursor on the final shape and size distribution of PdNPs synthesized via mechanochemical milling. A mixture of $PdCl_2$ and lignin powder which acts as the reductant and two stainless steel balls were added into a milling jar, and then the jar was placed onto the mixer mill which operated at a frequency of 29.5 Hz for 90 min. After finishing the process, the precipitate was scraped, washed and, finally, dried under vacuum. The resultant nanostructure included irregular-shaped PdNPs which were non-uniformly dispersed outside the lignin matrix. However, by replacing $PdCl_2$ with metal–organic precursors such as palladium (II) acetate and palladium (II) acetylacetonate, PdNPs transformed to more uniformly distributed spheres. Moreover, the PdNPs were distributed entirely within the matrix due to the excellent integration of precursor into the non-polar lignin structure.

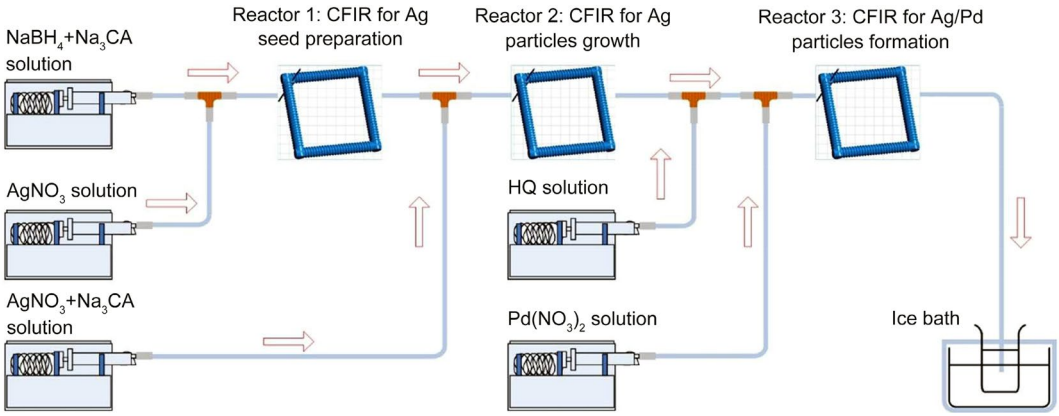

Fig. 11 Simple presentation of various synthesis steps of hollow Ag–Pd bimetallic NPs through galvanic replacement and coreduction in CFI reactors [153]

4 Metal rhenium nanoparticles

ReNPs and its compounds possess unique physiochemical properties such as good mechanical properties, refractoriness, and chemical inertness against some gasses, making them promising materials for nanoelectrode [158], SERS [159], sensor [160], and catalytic activities including isomerization [161], hydrogenation [162], and reduction [163]. However, compared to other transition metals, there are few papers reporting the synthesis of ReNPs, likely due to their high surface energy which could result in the oxidation of as-synthesized metallic ReNPs, [163]. Nonetheless, some techniques are developed which can effectively prevent the oxidation. These synthesis methods are summarized in Table 3.

4.1 Pure rhenium nanoparticles

Chemical reduction is the most common approach to produce ReNPs [181]. Mucalo et al. [164] performed hydrazine reduction of K_2ReCl_6 in the presence of gum arabic or arabinogalactan to produce a colloidally stable suspension of ReNPs. However, the resulting hydrosols exhibited low stability in aqueous media, slowly dissolving in water and forming stable perrhenate ions. In another research, Yi et al. [165] used 3-octanol to reduce ammonium perrhenate (NH_4ReO_4) at 180 °C under ambient atmosphere to synthesize ReNPs. The resultant ultra-small ReNPs were tested as acceptorless dehydrogenation (AD) catalysts. It was demonstrated that these ReNPs could transform secondary and benzylic alcohols to ketones and aldehydes, respectively. In another research, ^{60}Co γ-source irradiation was employed to reduce Re ions inside a reverse micelle solution [166]. Polar core of the micelles created an organized medium which facilitated the formation of ReNPs. Moreover, these micelles restricted the growth of ReNP, resulting in a reduction of the NP size. By employing a similar approach, Pd-Re bimetallic NPs were synthesized as well. Vollmer et al. [162] used 10 W microwave irradiation to reduce rhenium carbonyl ($Re_2(CO)_{10}$) in 1-butyl-3-methylimidazolium tetrafluoroborate (BMIM-BF_4) under an Ar atmosphere without any extra reductant and stabilizer. This process greatly simplified and accelerated the production of ReNPs by chemical reduction [167].

ReNPs can also be synthesized in water-in-oil (W/O) microemulsions of the metal salt and a reducing agent. By mixing these two microemulsions, the reactants collide due to the Brownian motion, resulting in fusion and reaction between reactants leading to the formation of metal nuclei [182]. Bedia et al. [168] produced ReNPs through both chemical reduction and microemulsion techniques. In the former, PVP was added to an aqueous precursor solution of K_2ReCl_6 or NH_4ReO_4, and then the mixed solution's temperature was adjusted between 10 and 80 °C. Finally, $NaBH_4$ was admixed as the reducing agent. The microscopic analysis of NPs showed that the increase of temperature resulted in fast reduction reaction, large mean size of NPs, and broad size distribution. Moreover, the slow addition of $NaBH_4$ could result in a narrow size distribution and a small average size. In another microemulsion synthesis process, two W/O microemulsion systems (*n*-heptane/sodium bis(2-ethylhexyl) sulfosuccinate (AOT)) of K_2ReCl_6 and $NaBH_4$ were mixed, and then placed into a rotary evaporator at 65 °C under vacuum to produce ReNPs. It showed that the high AOT concentration produced large ReNPs. Gyger et al. [169] developed a reverse microemulsion technique for ReNPs synthesis. Ammonia in oil microemulsion (a/o microemulsion) was formed by mixing heptane as the polar phase, dimethyldioctylammonium bromide or iodide (DDAB or DDAI) as cationic surfactant, and hexyl or heptyl amine as the co-surfactant in an emulsion with the ammonia to surfactant ratio up to 22.

Table 3 Various ReNPs synthesis techniques

NP type	Synthesis method	Function	Size (nm)	Shape	References
ReNPs	Chemical reduction	–	200–300	Sphere	[164]
Ultra-small ReNPs	Alcohol-assisted reduction	Acceptorless dehydrogenation of alcohols	2	Sphere	[165]
ReNPs	Radiation chemical reduction	–	2.5–4.5	Sphere	[166, 167]
Re-Pd bimetallic NPs			1.33		
ReNPs	Microwave irradiation-assisted reduction	Hydrogenation nanocatalysts for cyclohexene	0.8–5.0	Sphere	[162]
ReNPs	Chemical reduction	–	0.7–2.8	Sphere	[168]
	Microemulsion		0.8–1.4		
ReNPs	Microemulsion	–	1–8	Sphere	[169]
ReNPs	Thermal decomposition	Hydrogenation of difficult functional groups	1.0–1.2	Sphere	[170]
MPA-coated ReNPs and graphite-coated ReNPs	Pulsed laser decomposition	Catalyzing isomerization of 10-undecen-1-ol to internal alkenols	20–70	Sphere	[161]
ReNWs	Directional solidification and selective etching	Potential nanoelectrode for high-temperature measurements	400–1000 (diameter)	Fiber	[158, 171–173]
Ultra-small ReNPs@PAH	Chemical reduction	Catalyst for 4-NA reduction and SERS for MB probes	0.7 ± 0.25 1.7 ± 0.30	Sphere	[174]
Ultra-small ReNPs@DNA	Chemical reduction	Catalyst for 4-NA, 4-NP, and 2-NP reduction, and SERS for MB molecules	0.7 ± 0.1 1.1 ± 0.1	Sphere	[163]
Ultra-small ReNPs@DNA	Chemical reduction	Catalyst for hexavalent chromium ions reduction, and SERS for MB molecules	1.5 ± 0.7 6.5 ± 1.5	Sphere	[175]
Re@PE nanocomposites	Thermal decomposition	–	15.0 ± 0.3	Sphere	[41]
Re@PTFE nanocomposites	Thermal decomposition	–	5–30	Sphere	[176]
Re@MWCNTs nanocomposites	Wet impregnation	Catalysts or gas/liquid sensor	10–25 (diameter)	Fiber	[160, 177]
Re/MC	Wet impregnation	Hydrogenation of succinic acid to tetrahydrofuran	3.9–27.8	Sphere	[178]
Re@Graphite nanocomposites	Solid-state thermolytic demixing	Synthesis of high index facet SERS active NPs	3	Sphere	[159]
Re-NPC/a-C clusters	Solvothermal	HER catalysts	200–500	Berry-shape	[179]
Re/OMC	Solvent-evaporation induced self-assembly	Catalyst for the reduction of ANCs	2–5	Sphere	[180]

ReNWs rhenium nanowires, *4-NA* 4-nitroaniline, *MB* methylene blue, *HER* hydrogen evolution reaction, *ANCs* aromatic nitro compounds, *PTFE* polytetrafluoroethylene, *MPS* 3-mercaptopropionic acid, *DNA* deoxyribonucleic acids, *PAH* polyallylamine hydrochloride, *MWCNTs* multiwalled carbon nanotubes, *MC* mesoporous carbon, *a-C* amorphous carbon, *OMC* ordered mesoporous carbon

ReNPs are also produced by thermolysis of various Re complexes. Ayvalı et al. [170] synthesized ReNPs by decomposition of the dirhenium (II) tetraallyl complex $[Re_2(C_3H_5)_4]_{12}$ at 120 °C under H_2 in anisole as a solvent and either PVP or hexadecylamine (HDA) as the stabilizer. As the resultant ReNPs were partially oxidized under oxygen, the microstructure included an amorphous oxide shell embracing the metallic core. In another research, Chong et al. [161] employed pulsed-laser decomposition to make Re-based catalysts through photodecomposition using either NH_4ReO_4 or $Re_2(CO)_{10}$ as the precursor and MPA as the capping agent. The same technique was used to synthesize graphite-coated ReNPs by replacing MPA with triphenylphosphine (PPh_3).

Metallic nanowires (NWs) are essential components of various kinds of electrodes and are produced via different chemical plating or template-assisted electrochemical deposition [183]. However, template-based techniques suffer from interface reaction and structural damage during template detachment [184]. Hence, Hassel et al. [158] synthesized Re nanowires (ReNWs) through directional solidification and selective etching of a NiAl-1.5 at.%Re eutectic alloy using three oxidizing solutions: 3.2% HCl and 3% H_2O_2 in distilled water, 5 mol·L^{-1} sulphuric acid, or aqua regia. The

final structure of the matrix and the embedded nanowires were determined by the choice of oxidizing solution. Etching with the HCl/H_2O_2 mixture favored the production of long fibers and relatively few short rectangular fibers. Digestion in sulphuric acid produced long Re fibers with consistent shape and length. Treating samples with aqua regia caused the dissolution of two phases due to its high oxidizing power. Thermodynamic analysis illustrated that both the spacing and diameter of ReNWs increased with reducing the growth rate and temperature gradient, respectively [171]. Moreover, it was found that interface undercooling was also affected by the temperature gradient, suggesting temperature as an additional parameter to control the fiber spacing and diameter. Mechanical testing of ReNWs demonstrated the yield stress reached to a value between 10 and 60 GPA, which was ~ 10% of its Young's modulus and about 100 times higher than the one reported for its bulk form [172]. Increasing the diameters of ReNWs reduced their corresponding yield stress [173].

4.2 Rhenium-based nanocomposites

Kundu et al. [174] developed new Re-based catalysts on PAH scaffolds by reduction of NH_4ReO_4 with $NaBH_4$. The catalytic rate of 1.52×10^{-1} min^{-1} was achieved for the reduction of 4-NA, which is the highest ever reported. In addition to exceptional catalytic activity, the resultant self-assembled ultra-small ReNPs on the PAH chain formed

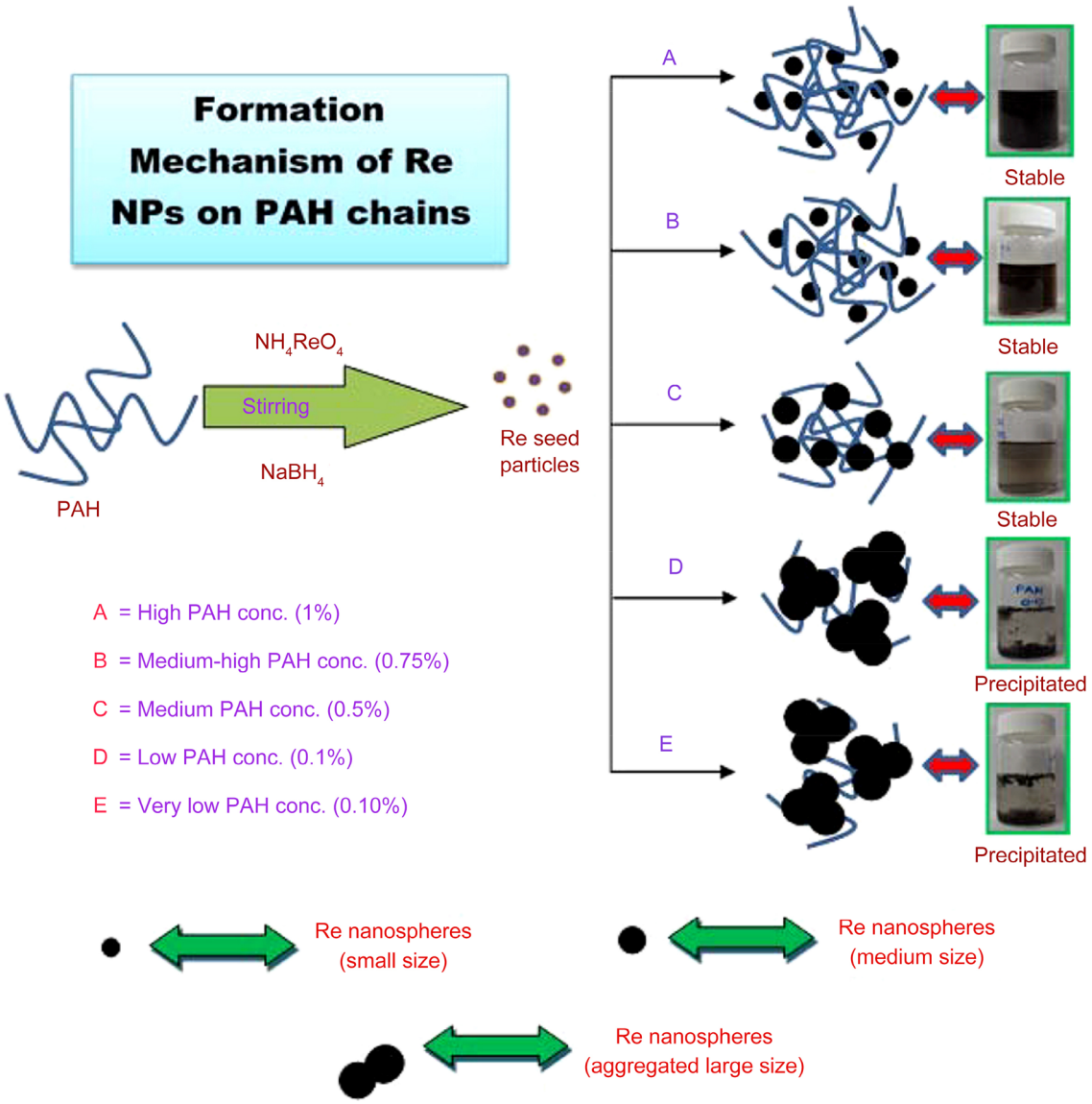

Fig. 12 Simple presentation of self-assembled ultra-small rhenium nanoparticles (USReNPs) formation on PAH scaffold and the effect of PAH concentration on the USReNPs size and behavior. Reproduced with permission from Ref. [174] Copyright 2017 American Chemical Society

abundant surface-active hot spots for SERS, and were used to detect MB. It showed that in the synthesis process, as the PAH concentration decreased from 1% to 0.5% the mean size of ReNPs increased (see Fig. 12). However, further lowering the PAH concentration to 0.1% or 0.01% would reduce the stability of NPs. Similarly, Anantharaj et al. [163] synthesized ultra-small ReNPs on deoxyribonucleic acid (DNA) scaffolds by the reduction of NH_4ReO_4 using borohydride as a reducing agent in the presence of DNA at room temperature. Like the previous report, varying the NH_4ReO_4:DNA molar ratio induced changes in the NP size. The superior catalytic efficiency of the ultra-small ReNPs@DNA hybrids was further confirmed for the reductions of 4-NP, 2-nitrophenol (2-NP), and 4-NA with respective reaction rate constant values of 6×10^{-2} min^{-1}, 33.83×10^{-2} min^{-1}, and 37.4×10^{-2} min^{-1}. The SERS study on detecting MB using such hybrids also demonstrated a high enhancement factor of 2.07×10^{7}. The same research group later synthesized ultra-small ReNPs in an organosol, where the mixture of NH_4ReO_4 and DNA was first transferred from the aqueous phase to the organic phase using tetraoctylammonium bromide (TOAB) as a phase transfer catalyst under freezing conditions and then reduced by $NaBH_4$ [175].

Yurkov et al. [41] employed a thermal decomposition approach to synthesize Re-polyethylene (Re@PE) nanocomposites. First, a mixture of PE and oil was heated under Ar flow. Concurrently, a rhenium-based compound such as NH_4ReO_4 in water, $Re_2(CO)_{10}$ in dimethylformamide (DMF), or $Re_4O_6(OCH_3)_{12}$ in absolute hexane was added to PE dropwise and the mixture decomposed at about 290 °C. Since the decomposition temperature of $Re_4O_6(OCH_3)_{12}$ (~ 140 °C) was much lower than the synthesis temperature (~ 290 °C), it completely decomposed, resulting in a high content of metallic Re. This group later utilized this approach to synthesize Re-based nanocomposites with PTFE instead of PE [176]. It was shown that low processing temperature resulted in both metallic and oxide phases of ReNPs with Re, ReO_2, and Re_2O_7.

ReNPs can also be integrated on various supports via wet impregnation. Dobrzańska-Danikiewicz et al. [160, 177] made gas or liquid sensors based on MWCNTs decorated with ReNPs. The MWCNTs were fabricated by catalytic chemical vapor deposition of C_2H_4 on a silicon substrate at 750 °C for 45 min. As the integration of ReNPs to the oxidized MWCNTs is stronger than that of pure MWCNTs, MWCNTs were functionalized by a treatment with concentrated HNO_3 in an ultrasound bath. Then, perrhenic acid ($HReO_4$) was added to the oxidized MWCNTs, and subsequently, nanotube impregnation was conducted by ultrasound sonication for 1 h followed by heating at 800 °C in a protected atmosphere of H_2 and Ar (see Fig. 13). Hong et al. [178] developed Re catalysts supported on MC. First, MC was prepared by a surfactant-templating technique. MC was by treated with different H_2SO_4 concentrations. Then, Re was applied to the MC support through a wetness impregnation process using an acetone solution of $ReCl_5$. Finally, the supported catalysts were calcined at 500 °C under nitrogen flow and dried overnight at 80 °C. The treatment of MC with a low concentration of H_2SO_4 resulted in little catalytic activity and using high concentration would destroy pore channels, so the optimal H_2SO_4 concentration must be tuned to optimize both catalytic activity and ReNP loading.

Recently, a solid-state surfactant-free approach was developed by Valenzuela et al. [159]. A mixture of $K[ReO_4]$ and cyclotriphosphazene $[NP(O_2C_{12}H_8)]_3$ was dissolved in dichloromethane, stirred for 24 h and dried. Then, it was heated to 300 °C first and then to 800 °C and kept for 2 h. The ReNPs were created through the demixing and nucleation of the metastable composite polymer. ReNPs crystallized across the cyclic phosphazene matrix which was also transformed to a solid graphitic carbon support during the pyrolysis step. The dispersion of supported ReNPs demonstrated high SERS signal for methyl violet 10B molecules.

In another research, Kim et al. [179] developed Re nanoparticle clusters (NPCs)-based catalysts for HER, where ReNPc was mixed with a-C which served as an electrically conductive material. ReO_2-NPC/a-Cs were synthesized in a two-step approach including the gelation of Re_2O_7 with tetrahydrofuran (THF) and the solovothermal processing of the formed gel. Afterwards, the resultant clusters were annealed at 500 °C for 4 h under Ar flow, which produced Re-NPc/a-Cs, as shown in Fig. 14. The berry-shaped Re-NPC/a-C clusters contained many catalytically active sites for HER, and the a-C phase provided the opportunity for a fast charge

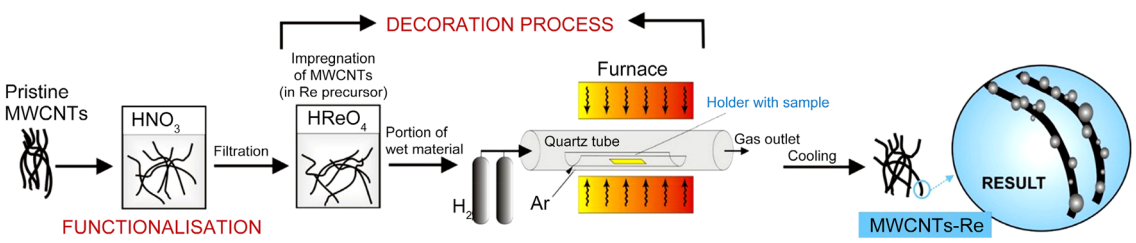

Fig. 13 Various synthesis steps of Re@MWCNT nanocomposites through the impregnation technique [177]

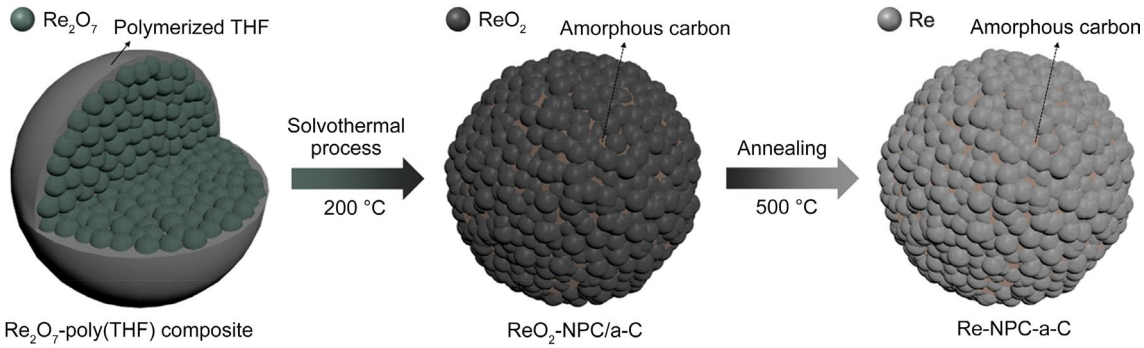

Fig. 14 Scheme of various synthesis stages of Re_2O_7-poly(THF), ReO_2-NPC/a-C, and Re-NPC/a-C berry shaped clusters. Reproduced with permission from Ref. [179] Copyright 2019 American Chemical Society

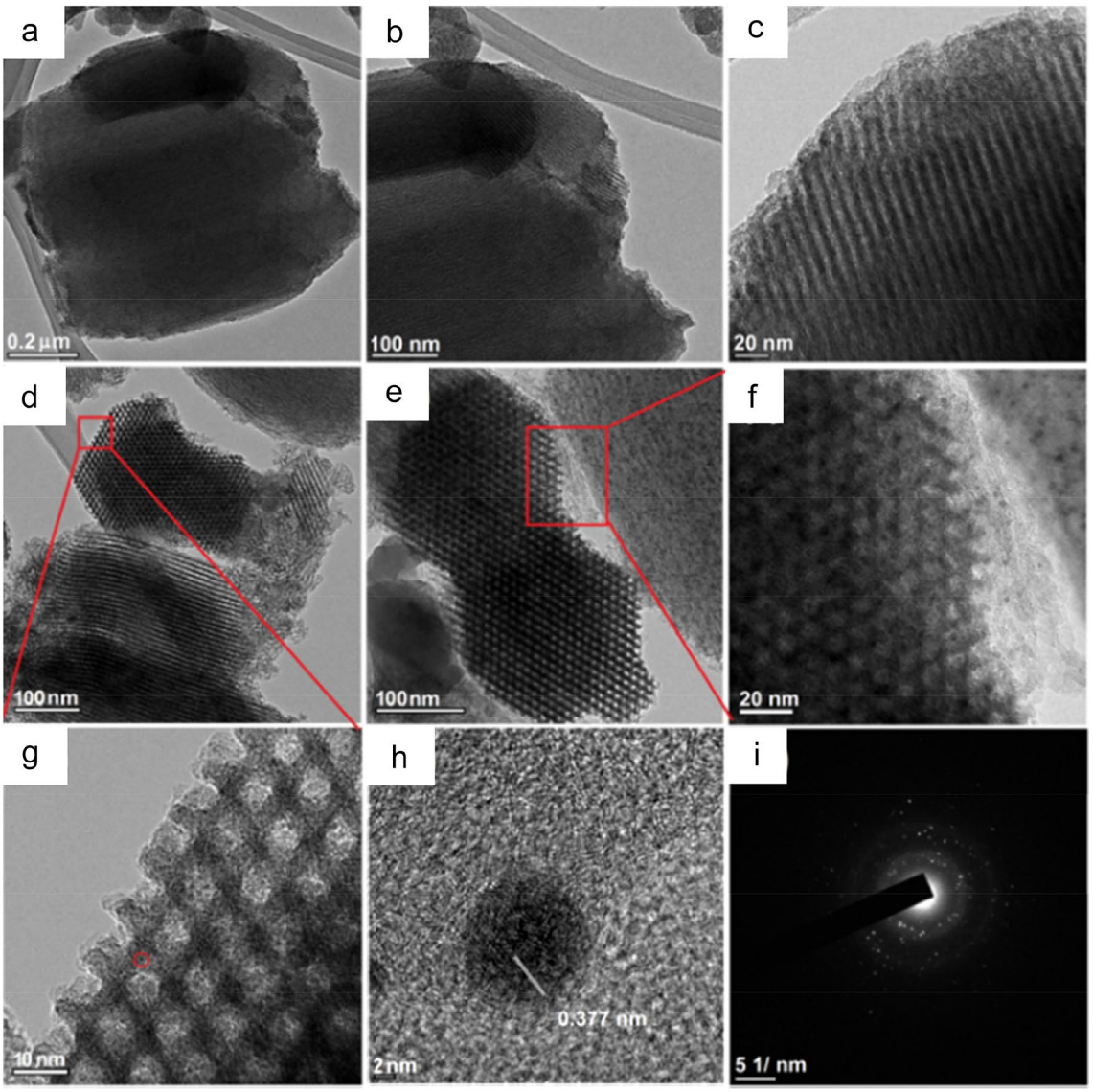

Fig. 15 FE-TEM micrographs of **a–c** bare OMC, **d–g** Re/OMC nanostructure, **h** single ReNP, and **i** the corresponding selected area electron diffraction (SAED) pattern of ReNPs. Reproduced with permission from Ref. [180] Copyright 2019 American Chemical Society

transfer. In yet another research, ReNPs were integrated on OMC via a solvent-evaporation induced self-assembly (EISA) method (see in Fig. 15) [180]. First, OMC was prepared by mixing of phloroglucinol-formaldehyde resol via EISA. Then, the resulting polymeric product was dissolved in a solution of $Re_2(CO)_{10}$ and THF. The polymeric gel was then cured at 80 °C under microwave irradiation followed by additional curing at 100 °C. During microwave irradiation, $Re_2(CO)_{10}$ was effectively converted to the Re^0 state and uniformly distributed on the 3D carbon support. The template was removed by carbonization at 400 °C under N_2 flow followed by a natural cooling process to achieve the final Re/OMC catalyst for the reduction of ANCs in aqueous media.

5 Conclusion

Today, nanotechnology plays a key role in varied scientific fields. Among them, MNPs have gained extensive interest due to their unique physiochemical properties originated from their nano-scale dimensions and structures which were governed by synthesis approaches. Here, we presented a detailed review of various chemical, physical, and biological synthesis methods for CoNPs, PdNPs, and ReNPs as well as their nanostructures and applications. CoNPs are synthesized using a wide range of methods, including chemical reduction, hydrogen reduction, hydrothermal, solvothermal, thermolysis, polyol, electrodeposition, liquid-phase plasma reduction, flame spray pyrolysis, ultrasonic spray pyrolysis, ion sputtering, ion implantation, arc discharge, pulsed laser ablation, and biogenic techniques. These CoNPs hare explored for very different applications, ranging from MRI contrast agents, antibacterial agents, chemical sensing, magnetic device, to catalysts for different chemical reactions. For PdNPs, synthesis techniques include chemical reduction, sonochemical, hydrothermal, electrodeposition, impregnation, combined hydrothermal and redox, polyol, seed-mediated growth, seed-etching, microwave irradiation-assisted reduction, pulsed laser ablation, microwave plasma torch, microwave-assisted polyol, mechanochemical milling, and biogenic approaches. PdNPs show promising potentials as SERS substrates, antibacterial agents, and catalyst for various reduction, oxidation, isomerization, and hydrogenation reactions. ReNP synthesis approaches include chemical reduction, alcohol-assisted reduction, microwave irradiation-assisted reduction, microemulsion, thermolysis, directional solidification and selective etching, impregnation, solid-state thermolytic demixing, solvothermal, solvent-evaporation induced self-assembly, and pulsed laser decomposition. Despite the limited research conducted with Re nanostructures, they already show immense promise in a wide range of catalytic applications such as for reduction, hydrogenation, HER, and isomerization reaction. At the same time, ReNPs also see the applications as SERS substrates and antibacterial agents.

In spite of significant progress in the synthesis of CoNPs, PdNPs, and ReNPs, there are still some roadblocks. Decreasing size distribution of pure metal nanoparticles, increasing dispersion homogeneity of nanoparticles through metal-based nanocomposites, and preventing nanoparticles agglomeration are main challenges for developing robust products for various applications. In addition, synthesis strategies should also be evaluated for their cost and the impact to the environment.

Acknowledgements This work was financially supported by National Institutes of Health (NIH) (Grant No. R15CA199019) and Cancer Prevention Research Institute of Texas (CPRIT) (Grant No. PR190678).

References

1. Feynman RP. There's plenty of room at the bottom. Caltech Eng Sci. 1960;23:22.
2. Khan I, Saeed K, Khan I. Nanoparticles: properties, applications and toxicities. Arab J Chem. 2019;12(7):908.
3. Auffan M, Rose J, Bottero JY, Lowry GV, Jolivet JP, Wiesner MR. Towards a definition of inorganic nanoparticles from an environmental, health and safety perspective. Nat Nanotechnol. 2009;4(10):634.
4. Jeevanandam J, Barhoum A, Chan YS, Dufresne A, Danquah MK. Review on nanoparticles and nanostructured materials: history, sources, toxicity and regulations. Beilstein J Nanotechnol. 2018;9(1):1050.
5. Vinci G, Rapa M. Noble metal nanoparticles applications: recent trends in food control. Bioengineering. 2019;6(1):10.
6. Neuschmelting V, Harmsen S, Beziere N, Lockau H, Hsu HT, Huang R, Razansky D, Ntziachristos V, Kircher MF. Dual-modality surface-enhanced resonance raman scattering and multispectral optoacoustic tomography nanoparticle approach for brain tumor delineation. Small. 2018;14(23):1800740.
7. Kvitek L, Prucek R, Panacek A, Soukupova J. Physicochemical aspects of metal nanoparticle preparation. In: Avramescu SM, Akhtar K, Fierascu I, Khan SB, Ali F, Asiri AM, editors. Silver nanoparticles, health and safety. London: IntechOpen; 2020. p. 213.
8. Bhattacharyya S, Kudgus RA, Bhattacharya R, Mukherjee P. Inorganic nanoparticles in cancer therapy. Pharm Res. 2011;28(2):237.
9. Sau TK, Rogach AL. Nonspherical noble metal nanoparticles: colloid-chemical synthesis and morphology control. Adv Mater. 2010;22(16):1781.
10. Li J, Zhao T, Chen T, Liu Y, Ong CN, Xie J. Engineering noble metal nanomaterials for environmental applications. Nanoscale. 2015;7(17):7502.
11. Jamkhande PG, Ghule NW, Bamer AH, Kalaskar MG. Metal nanoparticles synthesis: an overview on methods of preparation, advantages and disadvantages, and applications. J Drug Deliv Sci Technol. 2019;53:101174.
12. Rajput N. Methods of preparation of nanoparticles-a review. Int J Adv Eng Technol. 2015;7(6):1806.
13. Pacioni NL, Borsarelli CD, Rey V, Veglia AV. Synthetic routes for the preparation of silver nanoparticles. In: Alarcon EI, Griffith M, Udekwu KI, editors. Silver nanoparticle applications in

the fabrication and design of medical and biosensing devices. Linkoling: Springer; 2015. p. 13.
14. Ahmed S, Ahmad M, Swami BL, Ikram S. A review on plants extract mediated synthesis of silver nanoparticles for antimicrobial applications: a green expertise. J Adv Res. 2016;7(1):17.
15. Bucher J, Douglass D, Bloomfield L. Magnetic properties of free cobalt clusters. Phys Rev Lett. 1991;66(23):3052.
16. Wen S, Liu Y, Zhao X. The hierarchical three-dimensional cobalt superstructure: controllable synthesis, electromagnetic properties and microwave absorption. Adv Powder Technol. 2015;26(6):1520.
17. Yu Y, Mendoza-Garcia A, Ning B, Sun S. Cobalt-substituted magnetite nanoparticles and their assembly into ferrimagnetic nanoparticle arrays. Adv Mater. 2013;25(22):3090.
18. Alshammari A, Kalevaru VN, Martin A. Metal nanoparticles as emerging green catalysts. In: Larramendy ML, Soloneski S, editors. Green nanotechnology, overview and further prospects. London: IntechOpen; 2016. p. 2334.
19. Dey S, Dhal G. The catalytic activity of cobalt nanoparticles for low-temperature oxidation of carbon monoxide. Mater Today Chem. 2019;14:100198.
20. Den Breejen J, Radstake P, Bezemer G, Bitter J, Frøseth V, Holmen A, de Jong Kd. On the origin of the cobalt particle size effects in Fischer−Tropsch catalysis. J Am Chem Soc. 2009;131(20):7197.
21. Yang Y, Xu CL, Qiao L, Li XH, Li FS. Microwave magnetic properties and natural resonance of ε-Co nanoparticles. Chin Phys Lett. 2010;27(5):57501.
22. Narayanan T, Shaijumon M, Ajayan P, Anantharaman M. Synthesis of high coercivity cobalt nanotubes with acetate precursors and elucidation of the mechanism of growth. J Phys Chem C. 2008;112(37):14281.
23. Medvedeva O, Kambulova S, Bondar O, Gataulina A, Ulakhovich N, Gerasimov A, Evtugyn V, Gilmutdinov I, Kutyreva M. Magnetic cobalt and cobalt oxide nanoparticles in hyperbranched polyester polyol matrix. J Nanotechnol. 2017;7607658:1.
24. Leso V, Iavicoli I. Palladium nanoparticles: toxicological effects and potential implications for occupational risk assessment. Int J Mol Sci. 2018;19(2):503.
25. Iavicoli I, Bocca B, Carelli G, Caroli S, Caimi S, Alimonti A, Fontana L. Biomonitoring of tram drivers exposed to airborne platinum, rhodium and palladium. Int Arch Occup Environ Health. 2007;81(1):109.
26. Ravindra K, Bencs L, Van Grieken R. Platinum group elements in the environment and their health risk. Sci Total Environ. 2004;318(1–3):1.
27. Strobel R, Grunwaldt JD, Camenzind A, Pratsinis SE, Baiker A. Flame-made alumina supported Pd–Pt nanoparticles: structural properties and catalytic behavior in methane combustion. Catal Lett. 2005;104(1–2):9.
28. Wilson OM, Knecht MR, Garcia-Martinez JC, Crooks RM. Effect of Pd nanoparticle size on the catalytic hydrogenation of allyl alcohol. J Am Chem Soc. 2006;128(14):4510.
29. Semagina N, Renken A, Kiwi-Minsker L. Palladium nanoparticle size effect in 1-hexyne selective hydrogenation. J Phys Chem C. 2007;111(37):13933.
30. Dimitratos N, Porta F, Prati L. Au, Pd (mono and bimetallic) catalysts supported on graphite using the immobilisation method: synthesis and catalytic testing for liquid phase oxidation of glycerol. Appl Catal A. 2005;291(1–2):210.
31. Hou Z, Theyssen N, Brinkmann A, Leitner W. Biphasic aerobic oxidation of alcohols catalyzed by poly (ethylene glycol)-stabilized palladium nanoparticles in supercritical carbon dioxide. Angew Chem Int Ed. 2005;44(9):1346.
32. Narayanan R, El-Sayed MA. Carbon-supported spherical palladium nanoparticles as potential recyclable catalysts for the Suzuki reaction. J Catal. 2005;234(2):348.
33. Cheong S, Watt JD, Tilley RD. Shape control of platinum and palladium nanoparticles for catalysis. Nanoscale. 2010;2(10):2045.
34. da Silva FP, Fiorio JL, Rossi LM. Tuning the catalytic activity and selectivity of Pd nanoparticles using ligand-modified supports and surfaces. ACS Omega. 2017;2(9):6014.
35. Xia Y, Xiong Y, Lim B, Skrabalak SE. Shape-controlled synthesis of metal nanocrystals: simple chemistry meets complex physics. Angew Chem Int Ed. 2009;48(1):60.
36. Henry CR. Morphology of supported nanoparticles. Prog Surf Sci. 2005;80(3–4):92.
37. Ostroumov SA. Biological effects of surfactants. Boca Raton: Taylor & Francis; 2011. p. 255.
38. Azharuddin M, Zhu GH, Das D, Ozgur E, Uzun L, Turner AP, Patra HK. A repertoire of biomedical applications of noble metal nanoparticles. Chem Commun. 2019;55(49):6964.
39. Abdel-Karim R, Reda Y, Abdel-Fattah A. Nanostructured materials-based nanosensors. J Electrochem Soc. 2020;167(3):037554.
40. Naumov A. Rhythms of rhenium. Russ J Non-Ferrous Metals. 2007;48(6):418.
41. Yurkov GY, Kozinkin AV, Koksharov YA, Fionov AS, Taratanov NA, Vlasenko VG, Pirog IV, Shishilov ON, Popkov OV. Synthesis and properties of rhenium–polyethylene nanocomposite. Compos B Eng. 2012;43(8):3192.
42. Yao Y, Xu C, Qin J, Wei F, Rao M, Wang S. Synthesis of magnetic cobalt nanoparticles anchored on graphene nanosheets and catalytic decomposition of orange II. Ind Eng Chem Res. 2013;52(49):17341.
43. Mattila P, Heinonen H, Loimula K, Forsman J, Johansson LS, Tapper U, Mahlberg R, Hentze HP, Auvinen A, Jokiniemi J. Scalable synthesis and functionalization of cobalt nanoparticles for versatile magnetic separation and metal adsorption. J Nanopart Res. 2014;16(9):2606.
44. Varaprasad T, Govindh B, Rao B. Green synthesized cobalt nanoparticles using Asparagus racemosus root extract & evaluation of antibacterial activity. Int J ChemTech Res. 2017;10:339.
45. Silva LSd, Almeida FNCd, Moretti AL, Cher GG, Arroyo PA. Size control of cobalt nanoparticles through synthesis parameter variation. J Nanosci Nanotechnol. 2017;17(7):4704.
46. Cruz JC, Nascimento MA, Amaral HA, Lima DS, Teixeira APC, Lopes RP. Synthesis and characterization of cobalt nanoparticles for application in the removal of textile dye. J Environ Manag. 2019;242:220.
47. Kudlash A, Vorobyova S, Lesnikovich A. Interphase synthesis of colloidal magnetic cobalt nanoparticles. Magnetohydrodynamics. 2008;44(1):11.
48. Alex P, Majumdar S, Kishor J, Sharma IG. Synthesis of cobalt nano crystals in aqueous media and its characterization. Mater Sci Appl. 2011;2(9):1307.
49. Salman S, Usami T, Kuroda K, Okido M. Synthesis and characterization of cobalt nanoparticles using hydrazine and citric acid. J Nanotechnol. 2014;525193:1.
50. Swain B, Hong HS, Jung HC. Commercial process development for synthesis of spherical cobalt nanopowder by wet chemical reduction reaction. Chem Eng J. 2015;264:654.
51. Jang HD, Hwang DW, Kim DP, Kim HC, Lee BY, Jeong IB. Preparation of cobalt nanoparticles in the gas phase (I): Kinetics of cobalt dichloride reduction. J Ind Eng Chem. 2003;9(4):407.
52. Jang HD, Hwang DW, Kim DP, Kim HC, Lee BY, Jeong IB. Preparation of cobalt nanoparticles by hydrogen reduction of cobalt chloride in the gas phase. Mater Res Bull. 2004;39(1):63.
53. Dzidziguri EL, Sidorova EN, Inkar M, Yudin AG, Kostitsyna EV, Ozherelkov DY, Slusarsky KV, Nalivaiko AY, Gromov AA.

Cobalt nanoparticles synthesis by cobalt nitrate reduction. Mater Res Exp. 2019;6(10):105081.
54. Koskela P, Teirikangas M, Alastalo A, Forsman J, Juuti J, Tapper U, Auvinen A, Seppä H, Jantunen H, Jokiniemi J. Synthesis of cobalt nanoparticles to enhance magnetic permeability of metal–polymer composites. Adv Powder Technol. 2011;22(5):649.
55. Kim HG, Lee H, Kim BH, Kim SJ, Lee JM, Jung SC. Synthesis process of cobalt nanoparticles in liquid-phase plasma. Jpn J Appl Phys. 2013;52(1S):01AN03.
56. Seong G, Takami S, Arita T, Minami K, Hojo D, Yavari AR, Adschiri T. Supercritical hydrothermal synthesis of metallic cobalt nanoparticles and its thermodynamic analysis. J Supercrit Fluids. 2011;60:113.
57. Ansari S, Bhor R, Pai K, Sen D, Mazumder S, Ghosh K, Kolekar Y, Ramana C. Cobalt nanoparticles for biomedical applications: facile synthesis, physiochemical characterization, cytotoxicity behavior and biocompatibility. Appl Surf Sci. 2017;414:171.
58. Liu Q, Cao X, Wang T, Wang C, Zhang Q, Ma L. Synthesis of shape-controllable cobalt nanoparticles and their shape-dependent performance in glycerol hydrogenolysis. RSC Adv. 2015;5(7):4861.
59. Chen Z, Liu J, Evans AJ, Alberch L, Wei A. Calixarene-mediated synthesis of cobalt nanoparticles: an accretion model for separate control over nucleation and growth. Chem Mater. 2014;26(2):941.
60. Yang H, Su Y, Shen C, Yang T, Gao H. Synthesis and magnetic properties of ε-cobalt nanoparticles. Surf Interface Anal. 2004;36(2):155.
61. Bönnemann H, Brijoux W, Brinkmann R, Matoussevitch N, Waldöfner N, Palina N, Modrow H. A size-selective synthesis of air stable colloidal magnetic cobalt nanoparticles. Inorg Chim Acta. 2003;350:617.
62. Puntes VF, Zanchet D, Erdonmez CK, Alivisatos AP. Synthesis of hcp-Co nanodisks. J Am Chem Soc. 2002;124(43):12874.
63. Bao Y, An W, Turner CH. Krishnan KM The critical role of surfactants in the growth of cobalt nanoparticles. Langmuir. 2010;26(1):478.
64. Yadav M, Velampati RSR, Sharma R. Colloidal synthesized cobalt nanoparticles for nonvolatile memory device application. IEEE Trans Semicond Manuf. 2018;31(3):356.
65. Salavati-Niasari M, Fereshteh Z, Davar F. Synthesis of cobalt nanoparticles from [bis (2-hydroxyacetophenato) cobalt (II)] by thermal decomposition. Polyhedron. 2009;28(6):1065.
66. Sowka E, Leonowicz M, Andrzejewski B, Pomogailo A, Dzhardimalieva G. Cobalt nanoparticles processed by thermal decomposition of metal-containing monomers. Mater Sci-Wroclaw. 2006;24:311.
67. Gräf CP, Birringer R, Michels A. Synthesis and magnetic properties of cobalt nanocubes. Phys Rev B. 2006;73(21):212401.
68. Zola AS, Ribeiro RU, Bueno JMC, Zanchet D, Arroyo PA. Cobalt nanoparticles prepared by three different methods. J Exp Nanosci. 2014;9(4):398.
69. Schiavi PG, Altimari P, Pagnanelli F, Moscardini E, Toro L. Synthesis of cobalt nanoparticles by electrodeposition onto aluminium foils. Chem Eng Trans. 2015;43:673.
70. Grass RN, Stark WJ. Gas phase synthesis of fcc-cobalt nanoparticles. J Mater Chem. 2006;16(19):1825.
71. Grass RN, Athanassiou EK, Stark WJ. Covalently functionalized cobalt nanoparticles as a platform for magnetic separations in organic synthesis. Angew Chem Int Ed. 2007;46(26):4909.
72. Schumacher CM, Grass RN, Rossier M, Athanassiou EK, Stark WJ. Physical defect formation in few layer graphene-like carbon on metals: influence of temperature, acidity, and chemical functionalization. Langmuir. 2012;28(9):4565.
73. Gürmen S, Stopić S, Friedrich B. Synthesis of nanosized spherical cobalt powder by ultrasonic spray pyrolysis. Mater Res Bull. 2006;41(10):1882.
74. Shatrova N, Yudin A, Levina V, Dzidziguri E, Kuznetsov D, Perov N, Issi JP. Elaboration, characterization and magnetic properties of cobalt nanoparticles synthesized by ultrasonic spray pyrolysis followed by hydrogen reduction. Mater Res Bull. 2017;86:80.
75. Chung BX, Liu CP. Synthesis of cobalt nanoparticles by DC magnetron sputtering and the effects of electron bombardment. Mater Lett. 2004;58(9):1437.
76. Jacobsohn L, Hawley M, Cooke D, Hundley M, Thompson J, Schulze R, Nastasi M. Synthesis of cobalt nanoparticles by ion implantation and effects of postimplantation annealing. J Appl Phys. 2004;96(8):4444.
77. Attri A, Kumar A, Verma S, Ojha S, Asokan K, Nair L. Synthesis of cobalt nanoparticles on Si (100) by swift heavy ion irradiation. Nanoscale Res Lett. 2013;8(1):433.
78. El-Khatib AM, Badawi MS, Roston GD, Khalil AM, Moussa RM, Mohamed MM. Synthesis and characterization of cobalt nanoparticles prepared by arc discharge method using an ultrasonic nebulizer. J Nano Res. 2018;52:88.
79. Jyothi L, Kuladeep R, Rao DN. Solvent effect on the synthesis of cobalt nanoparticles by pulsed laser ablation: their linear and nonlinear optical properties. J Nanophoton. 2015;9(1):093088.
80. Yılmaz F, Lee DJ, Song JW, Hong HS, Son HT, Yoon JS, Hong SJ. Fabrication of cobalt nano-particles by pulsed wire evaporation method in nitrogen atmosphere. Powder Technol. 2013;235:1047.
81. Siada R. Green synthesized cobalt nano particles for using as a good candidate for sensing organic compounds. J Electrochem Sci Technol. 2015;6(4):111.
82. Igwe O, Ekebo E. Biofabrication of cobalt Nanoparticl odorata and their potentia. Res J Chem. 2018;8(1):11.
83. Ahmed K, Tariq I, Siddiqui SU, Mudassir M. Green synthesis of cobalt nanoparticles by using methanol extract of plant leaf as reducing agent. Pure Appl Biol. 2016;5(3):453.
84. Kim SC, Kim BH, Kim SJ, Lee YS, Kim HG, Lee H, Park SH, Jung SC. Preparation and characterization of cobalt/graphene composites using liquid phase plasma system. J Nanosci Nanotechnol. 2015;15(1):228.
85. Gubin S. Metalcontaining nano-particles within polymeric matrices: preparation, structure, and properties. Colloids Surf, A. 2002;202(2–3):155.
86. Gubin S, Spichkin YI, Koksharov YA, Yurkov GY, Kozinkin A, Nedoseikina T, Korobov M, Tishin A. Magnetic and structural properties of Co nanoparticles in a polymeric matrix. J Magn Magn Mater. 2003;265(2):234.
87. Wang X, Zhang F, Liu Y, Wang Z. Nitrogen-doped carbon nanotubes encapsulated cobalt nanoparticles hybrids for highly efficient catalysis of oxygen reduction reaction. J Electrochem Soc. 2018;165(15):J3052.
88. Liu Y, Dong P, Li M, Wu H, Zhang C, Han L, Zhang Y. Cobalt nanoparticles encapsulated in nitrogen-doped carbon nanotube as bifunctional-catalyst for rechargeable Zn-air batteries. Front Mater. 2019;6:85.
89. Guzmán MG, Dille J, Godet S. Synthesis of silver nanoparticles by chemical reduction method and their antibacterial activity. Int J Chem Biomol Eng. 2009;2(3):104.
90. Luidold S, Antrekowitsch H. Hydrogen as a reducing agent: state-of-the-art science and technology. JOM. 2007;59(6):20.
91. Kim HG, Lee H, Kim SJ, Kim DH, Kim JS, Kang SY, Jung SC. Synthesis of manganese nanoparticles in the liquid phase plasma. J Nanosci Nanotechnol. 2013;13(9):6103.
92. Rabenau A. The role of hydrothermal synthesis in preparative chemistry. Angew Chem, Int Ed Engl. 1985;24(12):1026.

93. Wu W, He Q, Jiang C. Magnetic iron oxide nanoparticles: synthesis and surface functionalization strategies. Nanoscale Res Lett. 2008;3(11):397.
94. Walton RI. Subcritical solvothermal synthesis of condensed inorganic materials. Chem Soc Rev. 2002;31(4):230.
95. Gurrappa I, Binder L. Electrodeposition of nanostructured coatings and their characterization—a review. Sci Technol Adv Mater. 2008;9(4):043001.
96. Rodriguez-Sanchez L, Blanco M, Lopez-Quintela M. Electrochemical synthesis of silver nanoparticles. J Phys Chem B. 2000;104(41):9683.
97. Majerič P, Friedrich B, Rudolf R. Au-nanoparticle synthesis via ultrasonic spray pyrolysis with a separate evaporation zone. Materiali Tehnologije. 2015;5(49):791.
98. Swihart MT. Vapor-phase synthesis of nanoparticles. Curr Opin Colloid Interface Sci. 2003;8(1):127.
99. Wei Q. Surface modification of textiles. 2009. Cambridge: Woodhead Publidhing Limited and CRC Press LLc. 164.
100. Akhtar MS, Panwar J, Yun YS. Biogenic synthesis of metallic nanoparticles by plant extracts. ACS Sustain Chem Eng. 2013;1(6):591.
101. Wu G, Johnston CM, Mack NH, Artyushkova K, Ferrandon M, Nelson M, Lezama-Pacheco JS, Conradson SD, More KL, Myers DJ. Synthesis–structure–performance correlation for polyaniline–Me–C non-precious metal cathode catalysts for oxygen reduction in fuel cells. J Mater Chem. 2011;21(30):11392.
102. Zou X, Huang X, Goswami A, Silva R, Sathe BR, Mikmeková E, Asefa T. Cobalt-embedded nitrogen-rich carbon nanotubes efficiently catalyze hydrogen evolution reaction at all pH values. Angew Chem Int Ed. 2014;53(17):4372.
103. Philippot K, Serp P. Concepts in nanocatalysis. Nanomater Catalysis. 2013;1:1.
104. Suzuki A. Carbon–carbon bonding made easy. Chem Commun. 2005;38:4759.
105. Reetz MT, De Vries JG. Ligand-free Heck reactions using low Pd-loading. Chem Commun. 2004;14:1559.
106. Yamauchi M, Ikeda R, Kitagawa H, Takata M. Nanosize effects on hydrogen storage in palladium. J Phys Chem C. 2008;112(9):3294.
107. Ye M, Gong J, Lai Y, Lin C, Lin Z. High-efficiency photoelectrocatalytic hydrogen generation enabled by palladium quantum dots-sensitized TiO_2 nanotube arrays. J Am Chem Soc. 2012;134(38):15720.
108. Zeng Q, Cheng JS, Liu XF, Bai HT, Jiang JH. Palladium nanoparticle/chitosan-grafted graphene nanocomposites for construction of a glucose biosensor. Biosens Bioelectron. 2011;26(8):3456.
109. Zhang Y, Xiang Q, Xu J, Xu P, Pan Q, Li F. Self-assemblies of Pd nanoparticles on the surfaces of single crystal ZnO nanowires for chemical sensors with enhanced performances. J Mater Chem. 2009;19(27):4701.
110. Gobal F, Faraji M. Electrodeposited polyaniline on Pd-loaded TiO2 nanotubes as active material for electrochemical supercapacitor. J Electroanal Chem. 2013;691:51.
111. Park JE, Park SG, Koukitu A, Hatozaki O, Oyama N. Effect of adding Pd nanoparticles to dimercaptan-polyaniline cathodes for lithium polymer battery. Synth Met. 2004;140(2–3):121.
112. Vishnukumar P, Vivekanandhan S, Muthuramkumar S. Plant-mediated biogenic synthesis of palladium nanoparticles: recent trends and emerging opportunities. ChemBioEng Rev. 2017;4(1):18.
113. Srimani D, Sawoo S, Sarkar A. Convenient synthesis of palladium nanoparticles and catalysis of Hiyama coupling reaction in water. Org Lett. 2007;9(18):3639.
114. Mazumder V, Sun S. Oleylamine-mediated synthesis of Pd nanoparticles for catalytic formic acid oxidation. J Am Chem Soc. 2009;131(13):4588.
115. Vancová M, Šlouf M, Langhans J, Pavlová E, Nebesářová J. Application of colloidal palladium nanoparticles for labeling in electron microscopy. Microsc Microanal. 2011;17(5):810.
116. Huang X, Zheng N. One-pot, high-yield synthesis of 5-fold twinned Pd nanowires and nanorods. J Am Chem Soc. 2009;131(13):4602.
117. Nemamcha A, Rehspringer JL, Khatmi D. Synthesis of palladium nanoparticles by sonochemical reduction of palladium (II) nitrate in aqueous solution. J Phys Chem B. 2006;110(1):383.
118. Qiu XF, Xu JZ, Zhu JM, Zhu JJ, Xu S, Chen HY. Controllable synthesis of palladium nanoparticles via a simple sonoelectrochemical method. J Mater Res. 2003;18(6):1399.
119. Li C, Sato R, Kanehara M, Zeng H, Bando Y, Teranishi T. Controllable polyol synthesis of uniform palladium icosahedra: effect of twinned structure on deformation of crystalline lattices. Angew Chem Int Ed. 2009;48(37):6883.
120. Garg G, Foltran S, Favier I, Pla D, Medina-Gonzalez Y, Gómez M. Palladium nanoparticles stabilized by novel choline-based ionic liquids in glycerol applied in hydrogenation reactions. Catal Today. 2019;346:69.
121. Chen YH, Hung HH, Huang MH. Seed-mediated synthesis of palladium nanorods and branched nanocrystals and their use as recyclable Suzuki coupling reaction catalysts. J Am Chem Soc. 2009;131(25):9114.
122. Niu W, Li ZY, Shi L, Liu X, Li H, Han S, Chen J, Xu G. Seed-mediated growth of nearly monodisperse palladium nanocubes with controllable sizes. Cryst Growth Des. 2008;8(12):4440.
123. Klinkova A, Larin EM, Prince E, Sargent EH, Kumacheva E. Large-scale synthesis of metal nanocrystals in aqueous suspensions. Chem Mater. 2016;28(9):3196–202.
124. Klinkova A, Cherepanov PV, Ryabinkin IG, Ho M, Ashokkumar M, Izmaylov AF, Andreeva DV, Kumacheva E. Shape-Dependent Interactions of Palladium Nanocrystals with Hydrogen. Small. 2016;12(18):2450.
125. Wei Z, Matsui H. Rational strategy for shaped nanomaterial synthesis in reverse micelle reactors. Nat Commun. 2014;5(1):1.
126. Yong P, Rowson NA, Farr JPG, Harris IR, Macaskie LE. Bioreduction and biocrystallization of palladium by Desulfovibrio desulfuricans NCIMB 8307. Biotechnol Bioeng. 2002;80(4):369.
127. Lengke MF, Fleet ME, Southam G. Synthesis of palladium nanoparticles by reaction of filamentous cyanobacterial biomass with a palladium (II) chloride complex. Langmuir. 2007;23(17):8982.
128. Manocchi AK, Horelik NE, Lee B, Yi H. Simple, readily controllable palladium nanoparticle formation on surface-assembled viral nanotemplates. Langmuir. 2010;26(5):3670.
129. Yang C, Manocchi AK, Lee B, Yi H. Viral-templated palladium nanocatalysts for Suzuki coupling reaction. J Mater Chem. 2011;21(1):187.
130. Nadagouda MN, Varma RS. Green synthesis of silver and palladium nanoparticles at room temperature using coffee and tea extract. Green Chem. 2008;10(8):859.
131. Lakshmipathy R, Reddy BP, Sarada N, Chidambaram K, Pasha SK. Watermelon rind-mediated green synthesis of noble palladium nanoparticles: catalytic application. Appl Nanosci. 2015;5(2):223.
132. Shaik MR, Ali ZJQ, Khan M, Kuniyil M, Assal ME, Alkhathlan HZ, Al-Warthan A, Siddiqui MRH, Khan M, Adil SF. Green synthesis and characterization of palladium nanoparticles using *Origanum vulgare* L. extract and their catalytic activity. Molecules. 2017;22(1):165.
133. Hazarika M, Borah D, Bora P, Silva AR, Das P. Biogenic synthesis of palladium nanoparticles and their applications as catalyst and antimicrobial agent. PLoS ONE. 2017;12(9):e0184936.

134. Kanchana A, Devarajan S, Ayyappan SR. Green synthesis and characterization of palladium nanoparticles and its conjugates from Solanum trilobatum leaf extract. Nano-micro Lett. 2010;2(3):169.
135. Eroglu E, ChenXJ, Bradshaw M, Agarwal V, ZouJL, Stewart SG, Duan XF, Lamb RN, Smith SM, Raston CL, Iyer KS. Biogenic production of palladium nanocrystals using microalgae and their immobilization on chitosan nanofibers for catalytic applications. RSC Adv. 2013;3(4):1009.
136. Petla RK, Vivekanandhan S, Misra M, Mohanty AK, Satyanarayana N. Soybean (Glycine max) leaf extract based green synthesis of palladium nanoparticles. J Biomater Nanobiotechnol. 2011;3:14.
137. Ullah S, Ahmad A, Khan A, Zhang J, Raza M, ur Rahman A, Tariq M, Zada S, Yuan Q. Palladium nanoparticles synthesis, characterization using glucosamine as the reductant and stabilizing agent to explore their antibacterial & catalytic applications. Microb Pathog. 2018;125:150.
138. Li G, Li Y, Wang Z, Liu H. Green synthesis of palladium nanoparticles with carboxymethyl cellulose for degradation of azodyes. Mater Chem Phys. 2017;187:133.
139. Gioria E, Wisniewski F, Gutierrez L. Microreactors for the continuous and green synthesis of palladium nanoparticles: enhancement of the catalytic properties. J Environ Chem Eng. 2019;7(3):103136.
140. Liu M, Wu L, Han J, Xu X, He C, Wang P, Wei Q, Yang W. Facile synthesis of palladium nanoparticles on hierarchical hollow silica spheres and its catalytic properties in Suzuki-reaction. R Soc Open Sci. 2018;5(9):180545.
141. Ko YJ, Kim JY, Lee KS, Park JK, Baik YJ, Choi HJ, Lee WS. Palladium nanoparticles from surfactant/fast-reduction combination one-pot synthesis for the liquid fuel cell applications. Int J Hydrogen Energy. 2018;43(41):19029.
142. Elazab HA, Moussa S, Gupton BF, El-Shall MS. Microwave-assisted synthesis of Pd nanoparticles supported on Fe_3O_4, Co_3O_4, and $Ni(OH)_2$ nanoplates and catalysis application for CO oxidation. J Nanopart Res. 2014;16(7):2477.
143. Li Y, Fan X, Qi J, Ji J, Wang S, Zhang G, Zhang F. Palladium nanoparticle-graphene hybrids as active catalysts for the Suzuki reaction. Nano Res. 2010;3(6):429.
144. Kakaei K, Gharibi H. Palladium nanoparticle catalysts synthesis on graphene in sodium dodecyl sulfate for oxygen reduction reaction. Energy. 2014;65:166.
145. Tang X, Haddad PA, Mager N, Geng X, Reckinger N, Hermans S, Debliquy M, Raskin J-P. Chemically deposited palladium nanoparticles on graphene for hydrogen sensor applications. Sci Rep. 2019;9(1):1.
146. Moussa S, Abdelsayed V, El-Shall MS. Laser synthesis of Pt, Pd, CoO and Pd–CoO nanoparticle catalysts supported on graphene. Chem Phys Lett. 2011;510(4–6):179.
147. Shim H, Phillips J, Fonseca I, Carabinerio S. Plasma generation of supported metal catalysts. Appl Catal A. 2002;237(1–2):41.
148. Chen W, Cai W, Lei Y, Zhang L. A sonochemical approach to the confined synthesis of palladium nanoparticles in mesoporous silica. Mater Lett. 2001;50(2–3):53.
149. Sun T, Zhang Z, Xiao J, Chen C, Xiao F, Wang S, Liu Y. Facile and green synthesis of palladium nanoparticles-graphene-carbon nanotube material with high catalytic activity. Sci Rep. 2013;3(1):1.
150. Dang-Bao T, Pradel C, Favier I, Gómez M. Bimetallic nanocatalysts in glycerol for applications in controlled synthesis. A structure–reactivity relationship study. ACS Appl Nano Mater. 2019;2(2):1033.
151. Asano S, Maki T, Sebastian V, Jensen KF, Mae K. Revealing the formation mechanism of alloyed Pd–Ru nanoparticles: a conversion measurement approach utilizing a microflow reactor. Langmuir. 2019;35(6):2236.
152. Cong C, Nakayama S, Maenosono S, Harada M. Microwave-assisted polyol synthesis of Pt/Pd and Pt/Rh bimetallic nanoparticles in polymer solutions prepared by batch and continuous-flow processing. Ind Eng Chem Res. 2018;57(1):179.
153. Wu KJ, Gao Y, Torrente-Murciano L. Continuous synthesis of hollow silver–palladium nanoparticles for catalytic applications. Faraday Discuss. 2018;208:427.
154. Rak MJ, Friščić T, Moores A. Mechanochemical synthesis of Au, Pd, Ru and Re nanoparticles with lignin as a bio-based reducing agent and stabilizing matrix. Faraday Discuss. 2014;170:155.
155. Karikalan N, Karthik R, Chen SM, Karuppiah C, Elangovan A. Sonochemical synthesis of sulfur doped reduced graphene oxide supported CuS nanoparticles for the non-enzymatic glucose sensor applications. Sci Rep. 2017;7(1):1.
156. Fiévet F, Ammar-Merah S, Brayner R, Chau F, Giraud M, Mammeri F, Peron J, Piquemal JY, Sicard L, Viau G. The polyol process: a unique method for easy access to metal nanoparticles with tailored sizes, shapes and compositions. Chem Soc Rev. 2018;47(14):5187.
157. Madigan MT, Martinko JM, Parker J. Brock biology of microorganisms. Upper Saddle River: Prentice Hall; 1997. p. 121.
158. Hassel AW, Rodriguez BB, Milenkovic S, Schneider A. Fabrication of rhenium nanowires by selective etching of eutectic alloys. Electrochim Acta. 2005;51(5):795.
159. Valenzuela CD, Valenzuela ML, Caceres S, O'Dwyer C. Solution and surfactant-free growth of supported high index facet SERS active nanoparticles of rhenium by phase demixing. J Mater Chem A. 2013;1(5):1566.
160. Dobrzańska-Danikiewicz AD, Łukowiec D, Wolany W. Comparative analysis of the structure of nanocomposites consisting of MWCNTs and Pt or Re nanoparticles. Carbon Nanotechnol. 2015; Manchester:One Central Press. 31.
161. Chong YY, Chow WY, Fan WY. Preparation of rhenium nanoparticles via pulsed-laser decomposition and catalytic studies. J Colloid Interface Sci. 2012;369(1):164.
162. Vollmer C, Redel E, Abu-Shandi K, Thomann R, Manyar H, Hardacre C, Janiak C. Microwave Irradiation for the Facile. Chem Eur J. 2010;16(12):3849.
163. Anantharaj S, Sakthikumar K, Elangovan A, Ravi G, Karthik T, Kundu S. Ultra-small rhenium nanoparticles immobilized on DNA scaffolds: an excellent material for surface enhanced Raman scattering and catalysis studies. J Colloid Interface Sci. 2016;483:360.
164. Mucalo MR, Bullen CR. Rhenium-based hydrosols: preparation and properties. J Colloid Interface Sci. 2001;239(1):71.
165. Yi J, Miller JT, Zemlyanov DY, Zhang R, Dietrich PJ, Ribeiro FH, Suslov S, Abu-Omar MM. A reusable unsupported rhenium nanocrystalline catalyst for acceptorless dehydrogenation of alcohols through γ-C–H activation. Angew Chem Int Ed. 2014;53(3):833.
166. Revina A, Kuznetsov M, Chekmarev A. Physicochemical properties of rhenium nanoparticles obtained in reverse micelles. Dokl Chem. 2013;450:119.
167. Revina A, Kuznetsov M, Chekmarev A, Boyakov E, Zolotarevskii V. Synthesis and physicochemical properties of rhenium nanoparticles. Protect Metals Phys Chem Surf. 2018;54(1):43.
168. Bedia J, Calvo L, Lemus J, Quintanilla A, Casas J, Mohedano A, Zazo J, Rodriguez J, Gilarranz M. Colloidal and microemulsion synthesis of rhenium nanoparticles in aqueous medium. Colloids Surf, A. 2015;469:202.
169. Gyger F, Bockstaller P, Gerthsen D, Feldmann C. Ammonia-in-oil-microemulsions and their application. Angew Chem Int Ed. 2013;52(47):12443.

170. Ayvalı T, Lecante P, Fazzini PF, Gillet A, Philippot K, Chaudret B. Facile synthesis of ultra-small rhenium nanoparticles. Chem Commun. 2014;50(74):10809.
171. Milenkovic S, Hassel AW, Schneider A. Effect of the growth conditions on the spatial features of Re nanowires produced by directional solidification. Nano Lett. 2006;6(4):794.
172. Philippe L, Peyrot I, Michler J, Hassel A, Milenkovic S. Yield stress of monocrystalline rhenium nanowires. Appl Phys Lett. 2007;91(11):111919.
173. Philippe L, Wang Z, Peyrot I, Hassel A, Michler J. Nanomechanics of rhenium wires: elastic modulus, yield strength and strain hardening. Acta Mater. 2009;57(14):4032.
174. Kundu S, Ma L, Dai W, Chen Y, Sinyukov AM, Liang H. Polymer encapsulated self-assemblies of ultrasmall rhenium nanoparticles: catalysis and SERS applications. ACS Sustain Chem Eng. 2017;5(11):10186.
175. Sakthikumar K, Anantharaj S, Ede SR, Karthick K, Kundu S. A highly stable rhenium organosol on a DNA scaffold for catalytic and SERS applications. J Mater Chem C. 2016;4(26):6309.
176. Taratanov N, Yurkov GY, Koksharov YA, Bouznik V. Preparation and properties of composite materials based on rhenium-containing nanoparticles and micrograins of polytetrafluoroethylene. Inorgan Mater Appl Res. 2011;2(2):118.
177. Dobrzańska-Danikiewicz AD, Wolany W, Łukowiec D, Jurkiewicz K, Niedziałkowski P. Characteristics of multiwalled carbon nanotubes-rhenium nanocomposites with varied rhenium mass fractions. Nanomater Nanotechnol. 2017;7:1847980417707173.
178. Hong UG, Park HW, Lee J, Hwang S, Yi J, Song IK. Hydrogenation of succinic acid to tetrahydrofuran (THF) over rhenium catalyst supported on H_2SO_4-treated mesoporous carbon. Appl Catal A. 2012;415:141.
179. Kim M, Yang Z, Park JH, Yoon SM, Grzybowski BA. Nanostructured rhenium-carbon composites as hydrogen-evolving catalysts effective over the entire pH Range. ACS Appl Nano Mater. 2019;2(5):2725.
180. Veerakumar P, Thanasekaran P, Lin KC, Liu SB. Well-dispersed rhenium nanoparticles on three-dimensional carbon nanostructures: efficient catalysts for the reduction of aromatic nitro compounds. J Colloid Interface Sci. 2019;506:271.
181. Soleimani Zohr Shiri M, Henderson W, Mucalo MR. A review of the lesser-studied microemulsion-based synthesis methodologies used for preparing nanoparticle systems of the noble metals, Os, Re, Ir and Rh. Materials. 2019;12(12):1896.
182. Zielińska-Jurek A, Reszczyńska J, Grabowska E, Zaleska A. Nanoparticles preparation using microemulsion systems. In: Najjar R, editor. Microemulsions-an introduction to properties and applications. Croatia InTech: Croatia; 2012. p. 229.
183. Zhao Z, Gao J, Wei L, Chui K. Tungsten wires and porous NiAl prepared through directional solidification and selective dissolution. Mater Manuf Process. 2017;32(16):1817.
184. Chen YH, Shen YM, Wang SC, Huang JL. Fabrication of one-dimensional ZnO nanotube and nanowire arrays with an anodic alumina oxide template via electrochemical deposition. Thin Solid Films. 2014;570:303.

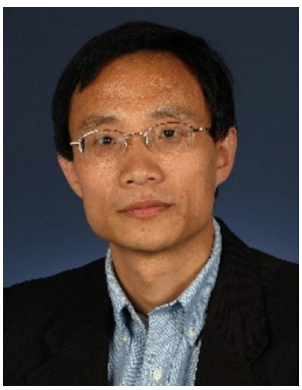

Dr. Yao-Wu Hao is a professor in the Department of Materials Science and Engineering at University of Texas at Arlington, USA. He received his Ph. D. degree from MIT in 2003 and his MS degree from University of Florida in 1998, both in Materials Science and Engineering. He was a postdoctoral fellow in the Department of Materials Science and Engineering at Johns Hopkins University before he joined UT Arlington in 2005. He earned Bachelor and Master of Science degrees in Metal Physics and Chemistry at the University of Science and Technology Beijing. His research focuses on synthesis, characterization and applications of metal and magnetic nanostructures.